Convergent close-coupling calculations of positron scattering from atomic carbon

N. A. Mori, L. H. Scarlett, I. Bray, and D. V. Fursa
Curtin Institute for Computation and Department of Physics and Astronomy, Curtin University, Perth, Western Australia 6102, Australia

(Received 27 September 2022; revised 3 January 2023; accepted 1 March 2023; published 17 March 2023)

We report on the extension of the single-center convergent close-coupling method to positron scattering on multielectron atoms, along with the development of a technique for separating the direct ionization and positronium-formation channels in single-center calculations. We have performed calculations of positron scattering on carbon and present total elastic, momentum transfer, excitation, direct ionization, total ionization, total inelastic, positronium-formation, stopping power, and total cross sections from threshold to 5000 eV. We also present oscillator strengths, the scattering length, the hidden Ramsauer-Townsend minimum, the energy of the positron-carbon virtual state, and the mean excitation energy. Agreement with electron-scattering experiment and positron-scattering theory for several cross sections has been demonstrated for high energies. However, discrepancies exist between different theoretical methods at lower energies and for the ionization and positronium-formation processes.

DOI: 10.1103/PhysRevA.107.032817

I. INTRODUCTION

Positrons have become a significant part of the medical industry in the past few decades due to their use in positron emission tomography (PET) scans and positherapy. PET scans have become critical in the fight against cancer as a noninvasive method of accurately imaging tumors inside the body [1]. They are also a powerful tool in biomedical research as they enable imaging of internal molecular processes occurring *in vivo* in real time [1,2]. PET scans can be used to investigate the pathogenesis of neurological disorders and diseases such as Alzheimer's and Parkinson's disease and could, in the future, allow for the monitoring and even presymptomatic diagnosis of these conditions [3]. Positherapy utilizes positrons to destroy cancer cells [4]. This treatment has proven useful in treating cancers where conventional methods are less effective since the preferential uptake of positron emitters by tumors as a result of their high metabolic rates leads to targeted internal radiotherapy [5–7]. Positherapy is a safer alternative to current radiotherapy approaches due to the rapid clearing of positron emitters from the body and the low range of the emitted positrons [8].

Both of these technologies function by introducing a radioactive tracer into the body, which produces high-energy positrons as it decays. These positrons release energy into the surrounding tissue, which in positherapy treatments results in cancer cell death. After losing sufficient energy, positrons undergo annihilation and release gamma rays which can be detected by PET scans and used to resolve an image of the internal biochemical processes occurring inside the body. Currently, however, quantifiable data on the exact scattering processes that occur between the emission and annihilation of these positrons are scarce and largely unknown [9]. These processes slow down the positron and eventually lead to it annihilating either directly or by first undergoing positronium formation, a reaction critical for PET scans as its decay emits 80% of detected gamma rays [10]. Accurate positron-scattering cross sections are required to calculate quantities such as positron energy deposition and range distributions in human tissue. These quantities can be used to model a positron's journey in positherapy treatments and increase the accuracy of PET scans, where uncertainty in the positron's range leads to image blur [11].

To calculate the cross sections for positron scattering on the complex molecules relevant in these processes, methods such as IAM [12,13], IAM-SCAR [14], IAM-SCAR + I [15], and Monte Carlo [16] rely on accurate cross sections for scattering on the atoms which compose them. One such atom is carbon, which constitutes approximately 18% of the human body and is a major component of biomolecules such as DNA.

Outside the medical industry, another area interested in positron-carbon scattering is tokamak reactor research since these reactors rely on materials containing carbon for their shielding and walls. Due to the large energies involved in fusion production, electron-positron pair production is a common event, and runaway positrons are created in large quantities [17,18]. Only 0.1% of these produced positrons annihilate within the plasma, with the rest colliding with the reactor wall [19].

A variety of different theoretical studies have been conducted for electron scattering on carbon, using the B-spline R matrix with pseudostates (BSR) [20,21], R matrix [22,23], R matrix with pseudostates (RMPS) [24], complex optical potential [25], momentum-space coupled-channels optical (CCO) [26], close-coupling (CC) [26,27], binary-encounter Bethe (BEB) [28,29], time-dependent close-coupling (TDCC) [24,30], and time-independent distorted-wave (TIDW) methods [24]. The only experimental data available for this system are the total ionization cross sections (TICS) measured by Brook *et al.* [31] and Wang and Crawford [32].

Studies for positron scattering have been less thorough, with fewer calculations previously attempted and no available measurements. Elastic and total cross sections (TCS) have been calculated between 100 and 5000 eV using a

model-potential approach by Reid and Wadehra [33]. Low-energy elastic scattering cross sections from 0 to 40 eV were calculated using variational methods by Malik [34] for the *s* wave. Elastic integrated and differential cross sections (DCS) for this system have also been calculated by Dapor and Miotello [35], Cai *et al.* [36], and Chaoui and Bouarissa [37], mainly for use in Monte Carlo simulations. Momentum transfer cross sections (MTCS) were determined for this purpose by Cai [38] and Dapor and Miotello [35]. Dapor and Miotello [35] performed these calculations by numerically solving the Dirac equation, Cai *et al.* [36,38] calculated cross sections using the ELSEPA code to also solve the Dirac equation [39], and Chaoui and Bourissa [37] numerically solved the Schrödinger equation. Although these previous calculations have been completed in both relativistic and nonrelativistic approaches, due to the low atomic number of carbon a nonrelativistic approach will suffice for the incident energies considered in this work.

Total cross sections have been evaluated from 1 to 5000 eV by Singh *et al.* [40] using a modified spherical complex optical potential (SCOP) method. Singh and Antony [41] followed this with calculations of positronium-formation along with total and direct ionization cross sections using a modified SCOP and the complex scattering potential–ionization contribution (CSP-ic) method. Stopping power values for this system have been presented by Gumus *et al.* [42] between 50 eV and 10 MeV using a generalized oscillator strength (GOS) model, earlier models used by Gumus *et al.* [42], the ICRU 37 report [43], and the PENELOPE program [44]. Another stopping power calculation for this system was undertaken by Ashley [45], who used an "optical-data" model to calculate results from 40 eV to 10 keV.

To date, the theoretical formulation of the convergent close-coupling (CCC) method has been limited to quasi-one- and -two-electron targets, those which can be described by one or two active electrons above an inert core, and hence has only been applied to positron scattering on hydrogen [46–48], helium [49–52], the alkali metals [53–56], and magnesium [57]. All of these calculations were conducted using either single- or two-center methods. In addition, positron scattering from noble gases was studied using CCC with a model accounting for one-electron excitations only [58]. As an *ab initio* approach which can be validated via convergence studies, the CCC method has proven useful in providing comprehensive data sets and verifying the theoretical and experimental results for these targets. Although theoretical results exist for positron scattering from carbon, these results are by no means extensive, with several important cross sections not present within the literature or only calculated above certain energies. Furthermore, calculations have only been conducted by one other method for many crucial cross sections. Consequently, this system will greatly benefit from large-scale accurate CCC calculations to verify the existing theory and reduce the gaps present in the literature.

We have extended the single-center CCC method to allow for complex structure models accounting for any number of active electrons with or without an inert core below them. This has been achieved using the MULT program developed by Zatsarinny [59] and the multiconfigurational Hartree-Fock (MCHF) code developed by Fischer [60]. We have utilized this modified CCC method to generate an accurate target structure model for C and perform close-coupling calculations for positron collisions with the carbon atom. We have produced a comprehensive cross-section data set for this system with incident energies between threshold and 5000 eV. To overcome the limitations of the single-center approach, we have developed a procedure utilizing a complex model potential that allows us to obtain estimates for positronium-formation and direct ionization cross sections. Atomic units are used throughout the paper unless otherwise stated.

II. CCC METHOD

The two-center close-coupling method is a rigorous approach to studying positron scattering from atomic or molecular targets. In this formulation, the total scattering wave function is expanded in terms of both target and positronium states. Although this approach allows explicit calculation of the direct ionization and positronium-formation cross sections, it is both computationally demanding and difficult to implement. To date, this approach has been applied to a few atoms (H, He, Mg, and several alkali metals) and a single molecule (H_2) [61,62].

A simpler alternative is the single-center approach, which utilizes a single expansion in terms of the target states. In this approach, positronium-formation channels are accounted for implicitly. The total ionization cross section contains contributions for single ionization from both direct ionization and positronium formation. The major limitations of this approach are the difficulty disentangling the direct ionization and positronium-formation processes and the issues arising due to mismatched boundary conditions between the positronium-formation and direct ionization thresholds. The single-center method for positron scattering is well documented in the literature for both atomic [46,51,52,56,58] and molecular targets [63,64], and hence here we only provide a summary of the method, with attention given to the modifications made to accommodate multielectron atoms in the CCC method. We also provide details on the implementation of the complex model optical potential technique [65] we have employed to address the aforementioned limitations of the single-center approach.

A. Atomic structure calculation

For an atomic target with N_e electrons and nuclear charge Z, the target Hamiltonian is given by

$$H_T = \sum_{i=1}^{N_e} \left(-\frac{1}{2}\nabla_i^2 - \frac{Z}{r_i} \right) + \sum_{i>j=1}^{N_e} \frac{1}{|\boldsymbol{r}_i - \boldsymbol{r}_j|}, \tag{1}$$

where $\boldsymbol{r}_i$ and $\boldsymbol{r}_j$ are the coordinates of electrons i and j. We utilize a configuration-interaction (CI) representation of the atomic wave functions:

$$\Phi_n^N(x_1, \ldots, x_{N_e}) = \sum_{i=1}^{N} C_i^{(n)} \phi_i(x_1, \ldots, x_{N_e}), \tag{2}$$

where ϕ_i are antisymmetrized N_e-electron configurations, $C_i^{(n)}$ are the CI coefficients, N is the number of configurations, and $x_i = (\boldsymbol{r}_i, \sigma_i)$ represents the spatial ($\boldsymbol{r}_i$) and spin (σ_i)

coordinates of electron i. The radial functions required for these configurations are either functions obtained from an MCHF calculation or the Laguerre basis functions

$$\varphi_{k\ell}(r) = \sqrt{\frac{\alpha_\ell (k-1)!}{(k+\ell)(k+2\ell)!}}(2\alpha_\ell r)^{\ell+1} \times e^{-\alpha_\ell r} L_{k-1}^{2\ell+1}(2\alpha_\ell r), \quad k = 1, \ldots, N_\ell. \tag{3}$$

Here, $L_{k-1}^{2\ell+1}$ are the associated Laguerre polynomials, α_ℓ are exponential falloff parameters, and N_ℓ is the number of functions for each ℓ.

The CI coefficients in Eq. (2) are obtained by diagonalizing H_T, and hence the pseudostates Φ_n^N satisfy

$$\langle \Phi_n^N | H_\mathrm{T} | \Phi_m^N \rangle = \epsilon_n^N \delta_{nm}, \tag{4}$$

where ϵ_n^N is the pseudostate energy. For sufficiently large N the low-lying states accurately represent true eigenstates, and the pseudostates form an arbitrarily complete basis for the target space.

B. Scattering calculation

The total scattering Hamiltonian for the positron-atom system is given by

$$H = H_\mathrm{T} - \tfrac{1}{2}\nabla_0^2 + V, \tag{5}$$

where index 0 represents the positron and V is the positron-atom interaction potential:

$$V = V_0 + \sum_{i=1}^{N_\mathrm{e}} V_{0i}. \tag{6}$$

Here, $V_0 = \frac{Z}{r_0}$ is the positron-nucleus potential and $V_{0i} = -\frac{1}{|r_0 - r_i|}$ are the positron-electron potential terms. We perform a multipole expansion of this potential, obtaining

$$V = 4\pi \sum_{\lambda,\mu} \frac{1}{2\lambda+1} \sum_{i=1}^{N_\mathrm{e}} v_\lambda(r_0, r_i) Y_{\lambda\mu}^*(\hat{\boldsymbol{r}}_0) Y_{\lambda\mu}(\hat{\boldsymbol{r}}_i), \tag{7}$$

where $Y_{\lambda\mu}$ are spherical harmonics, and

$$v_\lambda(r_0, r_i) = V_0 \delta_{\lambda 0} - \frac{[\min(r_0, r_i)]^\lambda}{[\max(r_0, r_i)]^{\lambda+1}}. \tag{8}$$

The Schrödinger equation for the total scattering wave function is given by

$$(H - E)|\Psi_i^{(+)}\rangle = 0, \tag{9}$$

where E is the energy of the collision system. In the single-center CCC method, Eq. (9) is solved by expanding $\Psi_i^{(+)}$ in the set of target pseudostates:

$$\Psi_i^{N(+)} = \sum_{n=1}^{N} F_n^{N(+)}(\boldsymbol{r}_0) \Phi_n^N(\boldsymbol{r}_1, \ldots, \boldsymbol{r}_{N_e}), \tag{10}$$

where $F_n^{N(+)}(\boldsymbol{r}_0)$ are the positron channel functions. This expansion is substituted into Eq. (9), which is then transformed into the coupled Lippmann-Schwinger equations for the T matrix:

$$\langle \boldsymbol{k}_f \Phi_f^N | T | \Phi_i^N \boldsymbol{k}_i \rangle = \langle \boldsymbol{k}_f \Phi_f^N | V | \Phi_i^N \boldsymbol{k}_i \rangle + \sum_{n=1}^{N} \int d\boldsymbol{k} \frac{\langle \boldsymbol{k}_f \Phi_f^N | V | \Phi_n^N \boldsymbol{k} \rangle \langle \boldsymbol{k} \Phi_n^N | T | \Phi_i^N \boldsymbol{k}_i \rangle}{E^{(+)} - \epsilon_n^N - \epsilon_k + i0}, \tag{11}$$

where $\epsilon_k = \frac{\boldsymbol{k}^2}{2}$ is the energy of the plane wave $|\boldsymbol{k}\rangle$. The use of plane waves assumes a neutral target; this method can be extended to charged targets by choosing a form of the asymptotic Hamiltonian that allows for scattering from ionic targets, and using Coulomb waves in place of plane waves. We perform a partial-wave expansion of the projectile plane waves and solve the Lippmann-Schwinger equations (11) per total scattering-system angular momentum J. For calculation of the V-matrix elements, we utilize a multipole expansion and standard angular momentum algebra to obtain the reduced matrix elements:

$$\begin{aligned}\langle kLM, \Phi_n^N; JM | V | k'L'M', \Phi_{n'}^N; J'M' \rangle &= \sum_\lambda \frac{4\pi}{2\lambda+1} \int_0^\infty u_L(kr_0) u_{L'}(kr_1) \langle L || Y_\lambda^*(\hat{\boldsymbol{r}}_0) || L' \rangle \\ &\times \delta_{J,J'} \delta_{M,M'} (-1)^{L+\ell'+2\lambda+J} \begin{Bmatrix} L' & \ell' & J \\ \ell & L & \lambda \end{Bmatrix} \\ &\times \langle \Phi_n^N || \sum_{i=1}^{N_\mathrm{e}} v_\lambda(r_0, r_i) Y_\lambda(\hat{\boldsymbol{r}}_i) || \Phi_{n'}^N \rangle, \end{aligned} \tag{12}$$

with $|kLM\rangle$ representing a partial wave with angular momentum L and angular-momentum projection M. Using the CI coefficients we have

$$\begin{aligned}\langle \Phi_n^N || \sum_{i=1}^{N_\mathrm{e}} v_\lambda(r_0, r_i) Y_\lambda(\hat{\boldsymbol{r}}_i) || \Phi_{n'}^N \rangle &= \sum_{mm'} C_m^{(n)} C_{m'}^{(n')} \langle \phi_m^n || \sum_{i=1}^{N_\mathrm{e}} v_\lambda(r_0, r_i) Y_\lambda(\hat{\boldsymbol{r}}_i) || \phi_{m'}^{n'} \rangle, \end{aligned} \tag{13}$$

where $C_m^{(n)}$ and $C_{m'}^{(n')}$ are the CI coefficients of the initial and final states, respectively, and the sums over m and m' cover all configurations. We then write

$$\begin{aligned}\langle \phi_m || \sum_{i=1}^{N_\mathrm{e}} v_\lambda(r_0, r_i) Y_\lambda(\hat{\boldsymbol{r}}_i) || \phi_{m'} \rangle &= \sum_{i=1}^{N_\mathrm{e}} a_i^{mm'} \int_0^\infty dr_i \, v_\lambda(r_0, r_i) \varphi_m(r_i) \varphi_{m'}(r_i), \end{aligned} \tag{14}$$

where φ_m are the radial functions obtained either from Eq. (3) or the MCHF calculations, and $a_i^{mm'}$ are coefficients which depend only upon the angular symmetry of the required configurations [59].

Since the potential V is real, we can solve Eq. (11) using real arithmetic by converting it into the equivalent equations for the K matrix [66]. An analytic Born completion technique [67] is also used to accelerate the convergence with respect to the size of the partial-wave expansion, as the Born approximation is accurate for high partial waves.

C. Mass stopping power

Previously, we have calculated mass stopping power for positron collisions with molecular hydrogen and its ion [63,68]. This is a useful quantity for mass transport studies which measure the positron energy loss per unit path length per unity density:

$$-\frac{1}{\rho}\frac{dE}{dx} \equiv Q_{\rm SP} = \frac{N_{\rm A}}{M}\sigma_{\rm SP}. \tag{15}$$

Here, $N_{\rm A}$ is Avogadro's number, x is the path length, ρ is the density of the target, M is the molar mass of the target, and $\sigma_{\rm SP}$ is the stopping power cross section. In the single-center CCC method $\sigma_{\rm SP}$ is obtained using

$$\sigma_{\rm SP} = \sum_{n=2}^{N}(\epsilon_n - \epsilon_1)\sigma_n, \tag{16}$$

where ϵ_n and σ_n are the energy and cross section of the nth electronic state, with $n = 1$ referring to the ground state. For our calculations, energy losses from direct annihilation have been omitted, but this cross section is expected to be small for the energies considered in this work.

A useful parameter that can be obtained directly from the stopping power is the mean excitation energy:

$$\overline{E} = \frac{\sigma_{\rm SP}}{\sigma_{\rm inel}}, \tag{17}$$

where $\sigma_{\rm inel}$ is the inelastic cross section, which is the sum of excitation, ionization, and positronium-formation cross sections. For simplicity, the dependence on the incident positron energy was removed from the above equations.

D. CCC calculation details

To begin, we utilize an MCHF C^+ calculation to obtain orbitals ranging from $1s$ to $5s$ that were optimized for the $2P^o$ ground state of this ion. All other orbitals are obtained via the Laguerre basis given in Eq. (3) with $N_\ell = 18 - \ell$, $\ell_{\rm max} = 8$, and $\alpha_\ell = 1.0$. The present close-coupling expansion includes the states of carbon derived from the configuration sets detailed here. The $2s^2 2pn\ell$ configurations were included for all orbitals up to $n = 18 - \ell$ with $\ell_{\rm max} = 8$. These configurations are important as all states derived from them are autoionizing [69], so their inclusion is necessary for a complete description of TICS. To account for the inner-core correlation, a set of different configurations had to be included in the structure model. These included $2s2pn\ell n'\ell'$ and $2s2pn\ell^2$ configurations, where $n\ell$ and $n'\ell'$ were all possible combinations of the $n = 3$, $n = 4$, and $5s$ orbitals. Also included were $2p^3 n\ell$ configurations for $n = 18 - \ell$ with $\ell \leqslant 2$. The first of these configurations has strong coupling with the states derived from $2s^2 2p^2$ [20]. Additionally, we included $2sn\ell^3$ configurations for $n\ell \leqslant 3d$. The $2p^4$ configuration was also included due to its strong mixing with the $1s2s^2 2p^2$ configuration [20]. To keep calculations at a reasonable size, the $2s2p^2 n\ell$ configurations were included only for $n = 18 - \ell$ with $\ell \leqslant 4$.

We included the first 943 out of 1797 target states generated using this basis in the close-coupling expansion, corresponding to those with excitation energies up to 40 eV above the ionization energy. Calculations were conducted for partial waves up to $J = 10$ for energies up to 5000 eV. A smaller close-coupling model was utilized to calculate elastic DCS for energies above 500 eV, as a large number of partial waves, even with the analytic Born completion technique, was required to obtain convergence in the DCS. This model was similar to the 943-state model but with the $2s2p^2 n\ell$ configurations limited to $n\ell \leqslant 5s$. Excitations were included only up to 25 eV above the ionization threshold, which generated a total of 379 states. Integrated elastic cross sections for this model and the 943-state model were converged within 2% for 500 eV and within 0.5% for energies above 1000 eV.

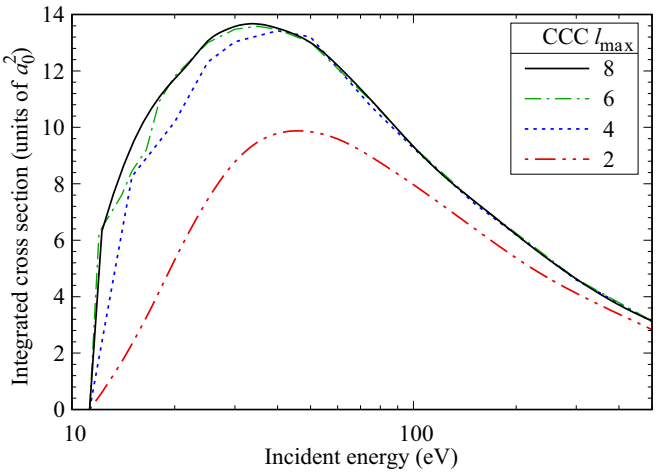

FIG. 1. CCC convergence study for total ionization cross section.

To obtain converged results for ionization, a 4571-state Born model with $\ell_{\rm max} = 8$ and a maximum n of 25 was also used. This model had a similar configuration structure as the previous model but with $2p^3 n\ell$ states for $n = 25 - \ell$ with $\ell \leqslant 6$ and with a $2s2p^2 n\ell$ continuum with $\ell_{\rm max} = 8$. Furthermore, all generated states were used, which included states with excitation energies up to 2057 eV above the ionization threshold. Using this model, we can approximate the contribution to the ionization cross section from states which were not included in the CCC calculation. Further details are given in Sec. IV B 4, where the extrapolation of the total ionization cross section is presented. This extrapolation is also present within the direct ionization and total cross sections as they are calculated from the extrapolated total ionization result.

The TCS was found to be converged for energies under 5 eV and above 18 eV for $\ell_{\rm max} \geqslant 6$, while the TICS is converged for energies higher than 20 eV for $\ell_{\rm max} \geqslant 6$. Convergence studies for the TICS are presented in Fig. 1 for the 575-state $\ell_{\rm max} = 2$, 834-state $\ell_{\rm max} = 4$, 901-state $\ell_{\rm max} = 6$, and 943-state $\ell_{\rm max} = 8$ calculations. The large differences for energies below 20 eV are representative of positronium formation as high-$\ell_{\rm max}$ values are necessary to accurately model positronium-formation channels in the single-center approach.

III. CCC-SCALED COMPLEX MODEL POTENTIAL METHOD

The single-center CCC method suffers from two drawbacks: the difficulty obtaining accurate cross sections between

the positronium-formation and ionization thresholds, and the difficulty disentangling the direct ionization and positronium-formation processes. To address these issues, we have developed a complex model-potential technique that uses the single-center approach. By scaling the model potential to fit results calculated with the single-center model, we obtain sufficiently reliable estimates for positronium-formation, direct ionization, and excitation cross sections between the positronium-formation and ionization thresholds. We provide a description of this technique here.

A. Complex model potential

The complex model-potential approach requires the calculation of a complex optical potential ($V_{\rm opt}$) given by

$$V_{\rm opt}(r, E_i) = V_{\rm st}(r) + V_{\rm pol}(r) + iV_{\rm abs}(r, E_i), \tag{18}$$

where $V_{\rm st}$ is the static interaction potential, $V_{\rm pol}$ is the polarization potential, $V_{\rm abs}$ is the absorption potential, and E_i is the incident positron energy. The absorption potential accounts for all inelastic processes.

The static potential $V_{\rm st}$ is calculated using [70]

$$V_{\rm st}(r) = \frac{Z}{r} - 4\pi\left(\frac{1}{r}\int_0^r dr'\rho(r')r'^2 + \int_r^\infty dr'\rho(r')r'\right), \tag{19}$$

where ρ is the electron density of the target obtained from the structure calculation. For calculation of $V_{\rm pol}$ we use

$$V_{\rm pol}(r) = -\frac{\alpha_{\rm D}}{2(r^2 + d^{\frac{1}{2}})^2}, \tag{20}$$

where $\alpha_{\rm D}$ is the static dipole polarizability of the target, and d is an adjustable parameter. The value of d is chosen for each energy so that the model potential produces the same elastic cross section as the CCC calculation. For the current calculation the values of this parameter are presented in Appendix D. We fit to a smooth interpolation of the single-center cross section for energies between the positronium-formation threshold and ionization threshold, where the CCC elastic cross section is unstable.

For the absorption potential we follow the method of Staszewska *et al.* [65], who give

$$V_{\rm abs}(r, E_i) = -\rho(r)\left[\sqrt{\frac{T_{\rm loc}}{2}}\left(\frac{8\pi}{10k_{\rm F}^3(r)E_i}\right) \times \theta\left[k_i^2 - k_{\rm F}^2(r) - 2\Delta\right](A_1 + A_2 + A_3)\right]. \tag{21}$$

Here, Δ is the absorption threshold, $k_{\rm F}(r)$ is the magnitude of the Fermi wave vector given by

$$k_{\rm F}(r) = [3\pi^2\rho(r)]^{\frac{1}{3}}, \tag{22}$$

and $\theta(x)$ is the Heaviside step function. Also present is the local kinetic energy of the projectile, which for positrons is given by

$$T_{\rm loc} = E_i - V_{\rm st}. \tag{23}$$

Finally, A_1, A_2, and A_3 are dynamic functions that rely on several of the above parameters. The equations for these functions are provided by Staszewska *et al.* [65] and are unmodified.

B. Delta variational technique

Positronium formation can not be explicitly included in the absorption potential formulation as this process can not be modeled by binary collisions [40]. Therefore to obtain the cross section for this transition, we utilize the delta variation technique, which modifies the absorption threshold Δ in Eq. (21). Several different versions of this modification exist in the literature [33,41,71]. To determine which formulation to use, we compared positronium-formation results for the H and He targets between this method and two-center CCC calculations. Based on these studies, we found the approach of Chiari *et al.* [71] most appropriate. Here, the absorption threshold is modified according to

$$\Delta(E) = \Delta_{\rm e} - (\Delta_{\rm e} - \Delta_{\rm p})e^{-(E_i - \Delta_{\rm p})/E_m}, \tag{24}$$

where $\Delta_{\rm e}$ and $\Delta_{\rm p}$ are the electronic-excitation and positronium-formation threshold energies, respectively. For the adjustable parameter E_m, Chiari *et al.* [71] used the energy for which $\sigma_{\rm inel}$ was found to have a maximum when not using the delta variation technique. However, we have used the energy at which the single-center CCC TCS has a maximum as this gave results for positronium formation in better agreement with two-center CCC results.

C. Scattering equations

To solve the scattering equations for the complex model potential, we employ a similar approach used in the CCC method by solving the Lippmann-Schwinger equations for a potential scattering system:

$$\langle \boldsymbol{k}_f|T|\boldsymbol{k}_i\rangle = \langle \boldsymbol{k}_f|V|\boldsymbol{k}_i\rangle + \int d\boldsymbol{k}\frac{\langle \boldsymbol{k}_f|V|\boldsymbol{k}\rangle\langle \boldsymbol{k}|T|\boldsymbol{k}_i\rangle}{k_i^2/2 - k^2/2 + i0}. \tag{25}$$

We perform a partial-wave expansion of the T- and V-matrix elements and integrate over the singularity at $k = k_i$, giving the partial-wave Lippmann-Schwinger equation

$$T_\ell(k_f, k_i) = V_\ell(k_f, k_i) + \mathcal{P}\int_0^\infty dk\frac{V_\ell(k_f, k)T_\ell(k, k_i)}{k_i^2/2 - k^2/2} - \frac{i\pi}{k_i}V_\ell(k_i, k_i)T_\ell(k_i, k_i), \tag{26}$$

where $\mathcal{P}$ indicates a principal-value integral. We discretize the k domain, and after some rearranging obtain

$$\sum_n(\delta_{f,n} - w_nV_{fn})T_{ni} = V_{fi}, \tag{27}$$

where $T_{fi} \equiv T_\ell(k_f, k_i)$, and w_n contain the integration weights and the denominator of the integrand for all off-shell k-grid points, while for the on-shell point it is

$$w_n = -\frac{i\pi}{k_n}. \tag{28}$$

By allowing f to run over the same range as n, i.e., all on- and off-shell k-grid points, we obtain a set of linear equations that can be solved to obtain the T-matrix elements. For this complex model potential calculation, the k domain was discretized into a total of 64 points following the standard approach detailed by Bray and Stelbovics [72], with convergence tested through calculations with larger number of points.

D. Cross-section evaluation and CCC scaling

Once the on-shell partial-wave T-matrix elements $T_\ell \equiv T_\ell(k_i, k_i)$ are obtained, the TCS is given by

$$\sigma_{\rm tot} = 4\pi^3 \sum_{\ell=0}^{\infty} (2\ell+1)|T_\ell|^2, \tag{29}$$

and applying the optical theorem, the elastic cross section is

$$\sigma_{\rm el} = -\frac{4\pi^2}{\sqrt{2E_i}} \sum_{\ell=0}^{\infty} (2\ell+1){\rm Im}(T_\ell). \tag{30}$$

The inelastic cross section, not including positronium formation, is then given by

$$\sigma_{\rm inel} = \sigma_{\rm tot} - \sigma_{\rm el}. \tag{31}$$

The positronium-formation cross section ($\sigma_{\rm Ps}$) is equal to the difference between the inelastic cross sections obtained from calculations with $\Delta(E) = \Delta_{\rm e}$ and $\Delta(E)$ given by Eq. (24). By comparing with two-center CCC results for positron scattering on H and He, we have found that this approach significantly underestimates the inelastic and positronium-formation cross sections. To correct this for systems where two-center calculations are not available, we scale the cross section for inelastic scattering minus positronium formation to reproduce the total cross section $\sigma_{\rm tot}$ obtained from the single-center CCC calculations at high energies. Following this, we scale the positronium-formation cross section $\sigma_{\rm Ps}$ to reproduce the single-center $\sigma_{\rm tot}$ at the maximum cross section between the ionization threshold and 10 eV above this threshold. Further details of this scaling procedure are provided in Appendix A.

We can disentangle the direct ionization by subtracting the calculated positronium-formation cross section from our TICS. We have done this for incident energies above 20 eV. To calculate direct ionization for energies below 20 eV, we have followed the CSP-ic method [73] and, using our results for positronium formation and direct ionization, have calculated the ratio

$$R(E_i) = \frac{\sigma_{\rm DI}}{\sigma_{\rm in}}, \tag{32}$$

where $\sigma_{\rm DI}$ is the direct ionization cross section and $\sigma_{\rm in}$ is the direct inelastic cross section, given by $\sigma_{\rm in} = \sigma_{\rm inel} - \sigma_{\rm Ps}$. The values for $\sigma_{\rm inel}$ are obtained directly from the single-center CCC calculation for $E > 20$ eV since the single- and two-center results for H and He were found to be in close agreement by 10 eV above the ionization threshold. Using a cubic spline, we extrapolate the calculated $R(E_i)$ down to the ionization threshold, where $R(E_i)$ is zero by definition. Following this we can obtain $\sigma_{\rm DI}$ for $E < 20$ eV by multiplying the $\sigma_{\rm in}$ calculated with the CCC-scaled complex model potential by $R(E_i)$. This process is illustrated in Appendix A.

IV. RESULTS

A. Structure

Excitation energies for C target states are presented in Table I for the 943-state CCC model and compared with the theoretical results of Wang *et al.* [21], Stancalie [23], Dunseath *et al.* [22], and NIST [74]. Differences between our calculated energies and NIST results range from 0.009 to 0.612 eV, with the difference generally increasing with increasing energy. The ionization limit from our structure model was within 0.04 eV of the NIST value. For the higher-energy states, our results are typically in-between the calculations of Dunseath *et al.* [22] and other calculations.

TABLE I. Excitation energies (eV) for C target states from the ground state, and the ionization limit.

	State	Term	CCC	Ref. [21]	Ref. [23]	Ref. [22]	NIST [74]
1	$2s^22p^2$	^3P	0.000	0.000	0.000	0.000	0.000
2	$2s^22p^2$	^1D	1.372	1.302	1.557	1.545	1.260
3	$2s^22p^2$	^1S	2.748	2.629	2.602	2.545	2.680
4	$2s2p^3$	$^5S^o$	3.940	3.963	3.092	3.133	4.179
5	$2s^22p3s$	$^3P^o$	7.617	7.527	7.401	8.488	7.481
6	$2s^22p3s$	$^1P^o$	7.818	7.750	7.740	8.936	7.680
7	$2s2p^3$	$^3D^o$	7.951	8.004	8.340	8.412	7.942
8	$2s^22p3p$	^1P	8.897	8.534	8.451	9.456	8.534
9	$2s^22p3p$	^3D	9.032	8.649	8.600	9.589	8.642
10	$2s^22p3p$	^3S	9.188	8.775	8.772	9.785	8.767
11	$2s^22p3p$	^3P	9.332	8.857	9.309	10.390	8.845
12	$2s2p^3$	$^3P^o$	9.481	9.379	9.517	9.981	9.326
13	$2s^22p3p$	^1D	9.553	9.014	9.443	10.757	8.998
14	$2s^22p3p$	^1S	9.766	9.172	10.424	11.370	9.168
15	$2s^22p3d$	$^1D^o$	10.166	9.614	9.772	10.719	9.627
16	$2s^22p4s$	$^3P^o$	10.258	9.673	10.142	10.810	9.683
17	$2s^22p3d$	$^3F^o$	10.271	9.687	9.517	10.809	9.695
18	$2s^22p3d$	$^3D^o$	10.288	9.705	9.607	10.888	9.705
19	$2s^22p4s$	$^1P^o$	10.301	9.685	9.549	10.834	9.709
20	$2s^22p3d$	$^1F^o$	10.333	9.716	9.607	10.947	9.732
21	$2s^22p3d$	$^1P^o$	10.370	9.748	9.653	10.970	9.758
22	$2s^22p3d$	$^3P^o$	10.404	9.840	13.407	11.018	9.830
Ion.	Limit		11.234				11.268
23	$2s2p^3$	$^1D^o$	13.600	12.968	14.470	14.645	
24	$2s2p^3$	$^3S^o$	13.279	13.073	13.407	15.366	13.117
25	$2s2p^3$	$^1P^o$	15.883	15.401	15.927	16.182	

Absorption oscillator strengths calculated in the 943-state CCC model are presented in Table II for three different lower-level states alongside the theoretical results of Wang *et al.* [21], Stancalie [23], Dunseath *et al.* [22], and NIST [74]. We find generally close agreement between our results and the results of Wang *et al.* [21] and NIST [74]; however, some notable disagreements are present for the $2s^22p3d\ ^1F^o$, $2s^22p3d\ ^3D^o$, and $2s^22p3d\ ^1P^o$ states where our calculations overestimate other results.

The convergence of the energy levels and oscillator strengths has been established by comparison between the 4571- and 943-state models. Differences between models were found to be under 1%. The dipole polarizability ($\alpha_{\rm D}$) of the 943-state model is 11.61 a_0^3, which is in close agreement with the 11.67 a_0^3 result of Das and Thakkar [75] and within 3% of the currently recommended value of 11.3 a_0^3 [76].

B. Scattering

1. Total

The present results for the TCS are compared with the calculations of Singh *et al.* [40] and Reid and Wadehra [33] in Fig. 2. Due to the mismatched boundary conditions with

TABLE II. Oscillator strengths for C.

Lower level	Upper level	CCC	Ref. [21]	Ref. [23]	Ref. [22]	NIST [74]
$2s^22p^2\ ^3P$	$2s^22p3s\ ^3P^o$	0.146	0.143	0.124	0.154	0.140
	$2s2p^3\ ^3D^o$	0.076	0.073	0.098	0.152	0.072
	$2s2p^3\ ^3P^o$	0.078	0.056	0.028	0.117	0.063
	$2s^22p4s\ ^3P^o$	0.037	0.027	0.023	0.010	0.021
	$2s^22p3d\ ^3D^o$	0.144	0.096	0.112	0.132	0.094
	$2s^22p3d\ ^3P^o$	0.037	0.037	0.340	0.069	0.040
	$2s2p^3\ ^3S^o$	0.143	0.156	0.171	0.269	0.152
$2s^22p^2\ ^1D$	$2s^22p3s\ ^1P^o$	0.118	0.103	0.128	0.103	0.118
	$2s^22p3d\ ^1D^o$	0.017	0.012	0.009	0.007	0.013
	$2s^22p4s\ ^1P^o$	0.015	0.007	0.004	0.010	0.011
	$2s^22p3d\ ^1F^o$	0.123	0.080	0.061	0.099	0.085
	$2s^22p3d\ ^1P^o$	0.011	0.011	0.018	0.014	0.009
	$2s2p^3\ ^1D^o$	0.256	0.224	0.344	0.529	
	$2s2p^3\ ^1P^o$	0.151	0.155	0.351	0.333	
$2s^22p^2\ ^1S$	$2s^22p3s\ ^1P^o$	0.088	0.090	0.021	0.0076	0.094
	$2s^22p4s\ ^1P^o$	0.008	0.011	0.007	0.001	0.005
	$2s^22p3d\ ^1P^o$	0.170	0.116	0.050	0.142	0.125
	$2s2p^3\ ^1P^o$	0.148	0.124	0.122	0.633	

channels corresponding to positive-energy pseudostates being closed while positronium-formation channels are open, accurate cross sections between the positronium-formation and ionization thresholds cannot be calculated with the single-center approach. To address this, we have utilized our CCC-scaled complex optical potential model to calculate the total cross section between the positronium-formation threshold and 20 eV. In this model, the direct inelastic component was scaled by a factor of 1.1 and the positronium formation by a factor of 2.91 to yield agreement with the CCC total cross section. We present this in the figure as CCC-pot, with results for all other energies in this model obtained from our single-center calculation. Following analysis of previous single- and two-center calculations, the single-center approach is believed to be sufficiently accurate for energies approximately 10 eV above the ionization threshold, which is why single-center CCC results are used for energies greater than 20 eV. We have also included in this figure the CCC results to demonstrate the difference between the ionization threshold and 20 eV. The CCC-pot cross section is larger for this energy range as it includes positronium formation, which cannot be adequately accounted for by the single-center model. For energies above 55 eV, the TICS component of the TCS is scaled according to the procedure detailed in Sec. IV B 4. Smooth cubic spline fitting has been applied for current results in all figures, except those presenting differential cross sections.

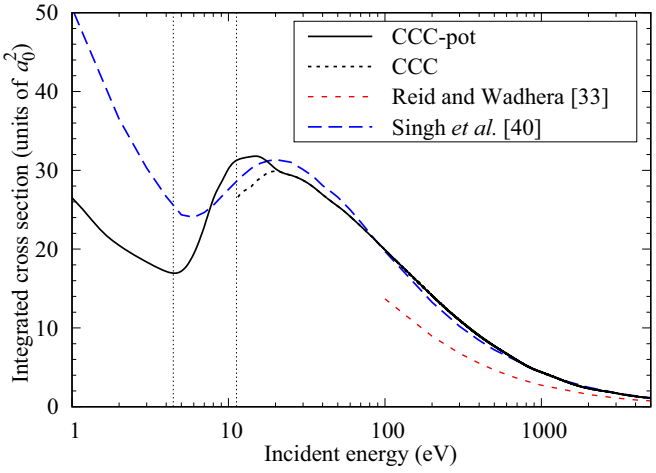

FIG. 2. Total cross section for positron scattering on carbon. CCC results are presented alongside theoretical results of Reid and Wadehra [33] and Singh *et al.* [40]. For energies between the positronium-formation threshold and 20 eV the CCC-pot results were calculated with the CCC-scaled complex model potential calculation. Below this threshold and above 20 eV the CCC-pot results are the same as the CCC. The vertical lines represent the positronium-formation and ionization thresholds.

Comparing our TCS to those of Singh *et al.* [40], we find good agreement above 70 eV and very close agreement above 800 eV. For energies between 18 and 70 eV, our results are slightly lower than those of Singh *et al.* [40], whereas from 7 to 18 eV, they are slightly larger. Below 7 eV, the CCC cross section is significantly lower than these results, most notably below the positronium-formation threshold of 4.46 eV. For this energy range, the only contribution to the TCS is the elastic cross section, and the CCC results are up to a factor of 2 lower than those of Singh *et al.* [40]. Below the positronium-formation threshold, the single-center approach gives practically exact results (as soon as convergence is established). Hence, this discrepancy indicates that the potential is too strong in the calculations of Singh *et al.* [40], resulting in a larger absolute value of the scattering length. Another aspect that differentiates the current method and that of Singh *et al.* [40] is that they do not account for virtual positronium formation. This is an important aspect of positron scattering at energies below the positronium-formation threshold. For example, in positron scattering from helium Gribakin and King [77] found that it accounted for 20% of the total correlation potential and that its inclusion was necessary to produce an accurate elastic cross section at low energies.

The TCS in both methods decreases from 1 eV to the positronium-formation threshold as a result of the decreasing elastic cross section. Above this threshold, as inelastic channels open, cross sections quickly rise to a maximum. This maximum cross section is predicted by the CCC and Singh *et al.* [40] to occur at approximately 20 eV, whereas the CCC-pot approach predicts the maximum at 15 eV. The model-potential calculations of Reid and Wadehra [33] were only conducted over an energy range of 100 to 5000 eV, and their cross section is lower than both the SCOP method of Singh *et al.* [40] and the single-center CCC approach.

2. Total ionization

For the total ionization cross section, which is equal to the sum of direct ionization and positronium formation, the current CCC results are compared with the results of Singh and Antony [41] and experimental results for the incident electron case [31,32] in Fig. 3. The CCC results predict a double maximum in the cross section, the first due to positronium formation and the second due to direct ionization. Of these, the first maximum has a larger magnitude. The results

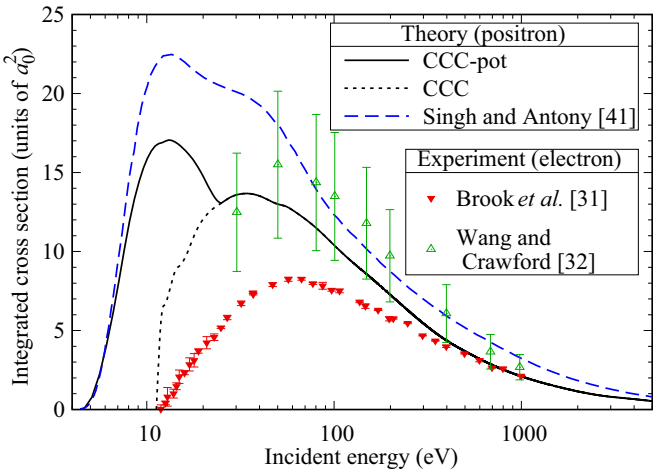

FIG. 3. Total ionization cross section of positron scattering on carbon from the positronium-formation threshold to 5000 eV. CCC-pot results are presented alongside CCC results, the theoretical results of Singh and Antony [41] and experimental results for electrons incident on carbon measured by Brook *et al.* [31] and Wang and Crawford [32].

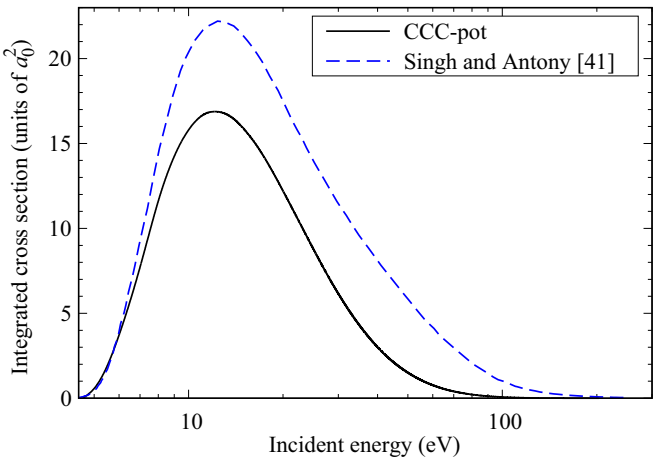

FIG. 4. Positronium-formation cross section for a positron incident upon carbon. CCC-pot results are presented alongside theoretical results of Singh and Antony [41].

of Singh and Antony [41] predict a much larger positronium-formation cross section than the direct ionization, leading to a less-pronounced shoulder due to direct ionization. The first maximum due to positronium formation occurs at 10 eV in both our CCC-pot calculation and the results of Singh and Antony [41]. Our method, however, predicts this maximum cross section to be almost 30% lower than that of Singh and Antony [41]. At high energies, electron and positron results are expected to be equal due to the exchange, Ps-formation, and interchannel coupling effects becoming negligible. For this scattering system, we see this occurs for TICS above 500 eV as the CCC results are within the experimental error of both electron experiments above this energy. Although in agreement for high energies, for lower energies large discrepancies exist between the electron results of Brook *et al.* [31] and Wang and Crawford [32]. The uncertainties of these two experiments are, however, significantly different with Wang and Crawford [32] measurements having an uncertainty of 30% whereas the uncertainty of Brook *et al.* [31] decreases with increasing energy, with an uncertainty of 9% at 20 eV decreasing to less than 2% by 1000 eV. The results of Singh and Antony [41] are significantly larger than the CCC-pot results for energies between 7 and 50 eV and are in disagreement with the electron experiment results at high energies. Further analysis of the discrepancies at high energies is provided later in our discussion of direct ionization in Sec. IV B 3.

As we consider incident energies up to 5000 eV, the ionization from the inner $1s$ shell becomes possible. We have performed Born calculations to determine the impact of ionization from this shell, which has an ionization threshold of approximately 300 eV. This calculation included $1s^1 2s^2 2p^2 n\ell$ configurations for $n \leqslant 25$ and $\ell \leqslant 8$ into our 4571-state Born model, which raised the total number of states to 6380. Comparing the TICS between this 6380-state and the 4571-state model, we found that the difference in TICS was within 1% from 300 to 5000 eV. Distorted-wave calculations for electron-impact ionization by Jonauskas [78] have also reported ionization from the $1s$ orbital to be insignificant. Hence, errors in our TICS from excluding ionization from this orbital are expected to be negligible for the considered energy range.

3. Positronium formation and direct ionization

Presented in Fig. 4 is the positronium-formation cross section calculated with our CCC scaled complex model potential approach alongside the calculations of Singh and Antony [41]. We find that the results of Singh and Antony [41] are significantly larger than the present calculation. Although their results are also from a complex model potential calculation, we are able to fit our results to accurate single-center calculations. The errors associated with this approach are analyzed in Appendix C for H and He targets. For energies below 33 eV, we expect errors of within 20% for the positronium-formation cross section, while for energies above this, we expect increasing errors with increasing energy. As σ_{Ps} rapidly decreases for higher energies, the impact of these larger errors will be minimal.

We present in Fig. 5 our current results for direct ionization alongside the theoretical results of Singh and Antony [41] and the measurements for the incident electron case from Brook *et al.* [31] and Wang and Crawford [32]. For direct ionization, the CCC-pot results are lower than those of Singh and Antony [41] above 20 eV, while good agreement is found below 20 eV down to the ionization threshold. Both calculations predict a cross-section peak at 60 eV. For energies above approximately 150 eV, direct ionization is by far the dominant component of the TICS; hence, the same observations at high energy can be made here as for TICS. The disagreement between the electron experiments of Brook *et al.* [31] with the results of Singh and Antony [41] at high energies is likely a result of the inaccuracies associated with the CSP-ic method, in which σ_{DI} is predicted from σ_{in} based on an expectation that σ_{DI} will be between 70%–80% of σ_{in} at its maximum, and 100% for large energies. From our calculations we predict the direct ionization cross section to be 66% of σ_{in} at the peak at 60 eV,

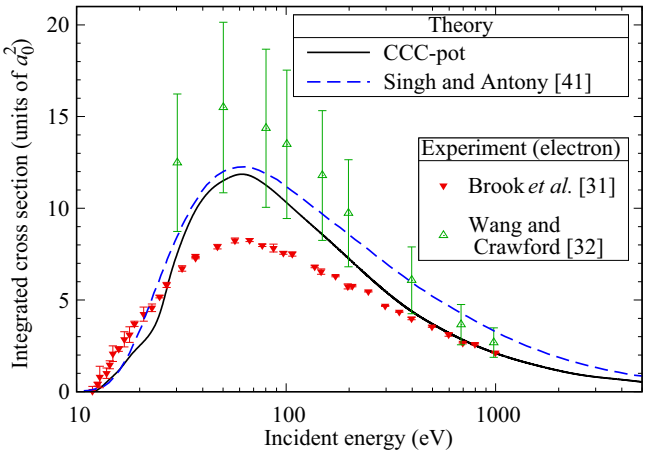

FIG. 5. Direct ionization cross section of positron incident upon carbon. Results calculated from our CCC-pot approach are presented alongside the theoretical calculation of Singh and Antony [41] and the experimental results for electrons incident on carbon measured by Brook *et al.* [31] and Wang and Crawford [32].

and by 5000 eV we find that ionization still only comprises 71% of σ_{in}.

4. Born extrapolation

Our total and direct ionization cross sections were extrapolated using the 4571-state Born calculation for energies above 55 eV. This was accomplished by multiplying the CCC results by the ratio between the 4571- and 943-state Born TICS. To confirm the validity of the 4571-state Born calculation, we utilized the scaling method developed by Kim [79] to compare TICS results with both electron experiments and BEB calculations [28], as shown in Fig. 6. For energies above 200 eV, the scaled Born results are within the error of the experiment by Brook *et al.* [31]. For the range 30 to 200 eV, these scaled Born results are marginally larger than this experiment, and

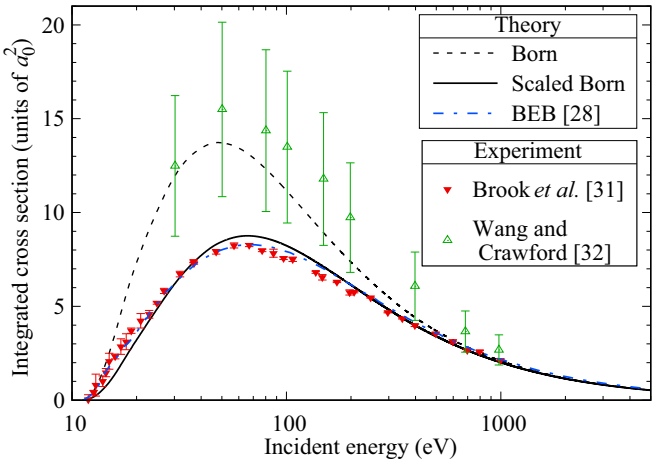

FIG. 6. 4571-state plane-wave Born calculations for the total ionization cross section of an electron scattering on carbon. Born calculations utilizing the scaling method of Kim [79] are also presented. These results are compared against the BEB calculations [28] and the experimental measurements by Brook *et al.* [31] and Wang and Crawford [32].

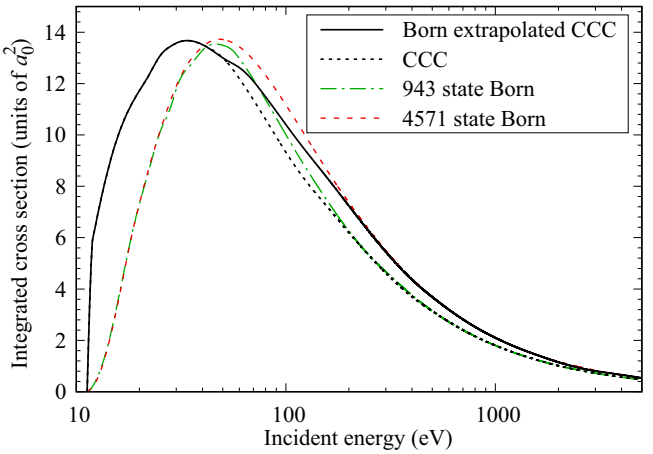

FIG. 7. 4571- and 943-state plane-wave Born alongside 943-state single-center CCC and Born extrapolated CCC results for the total ionization cross section of a positron incident upon carbon.

below 30 eV, they are somewhat lower. The unscaled results are significantly larger than this experiment for energies below 500 eV. Above 200 eV, the BEB results are in close agreement with the scaled Born results. The experimental results of Wang and Crawford [32] significantly overestimate the current and BEB results, with it in closer agreement with the Born result. The agreement for scaled Born results with the more accurate experiment of Brook *et al.* [31] and other theory provides direct evidence of the accuracy of our structure model.

In Fig. 7, we present the 943- and 4571-state Born calculations utilized for our extrapolation procedure, along with the single-center 943-state CCC result and the extrapolated cross section. The extrapolation has the greatest effect for energies between 100 and 1000 eV, with the Born and CCC results converged for energies above 300 eV. The 943-state model contains all excitations up to 40 eV above the ionization threshold. We can see this reflected in the figure, with the 4571- and 943-state models being in near perfect agreement up to 40 eV, in close agreement up to 60 eV, and then above 60 eV, the 4571-state model is noticeably larger. Using the Born extrapolation procedure, we can capture the states which become energetically accessible at incident energies above 52 eV without requiring close-coupling calculations, which would be unfeasible with this number of states.

5. Inelastic

In Fig. 8 we present the inelastic cross section. This result was calculated using the CCC-pot approach, with values above 20 eV obtained from the single-center CCC calculation and values below 20 eV calculated with the CCC-scaled complex model potential technique. Also included in this figure are the total excitation, direct ionization, and positronium-formation cross sections, which make up the total inelastic cross section. To reiterate, the positronium-formation results are obtained directly from the CCC-scaled complex model potential calculation. The direct ionization result is obtained from subtracting these results from the TICS, and using the CSP-ic method below 20 eV. As with the inelastic result, the total bound excitation is obtained below 20 eV with the CCC-scaled complex model potential and above from

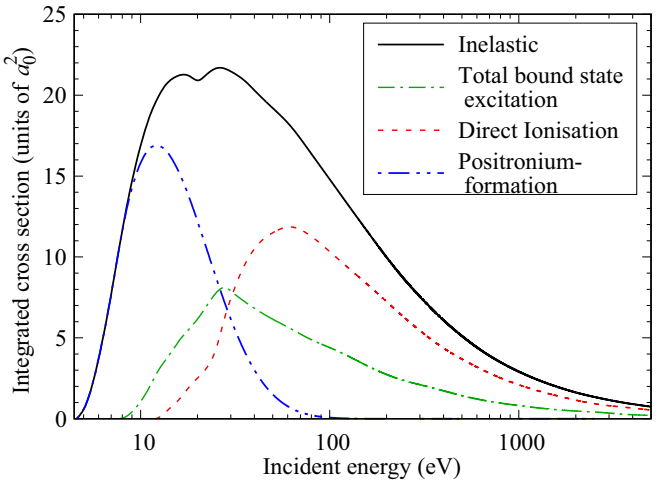

FIG. 8. The inelastic cross section and its components calculated through the combination of our single-center CCC and CCC-scaled complex model potential. Exact details are provided in the text. Results are presented from the positronium-formation threshold to 5000 eV.

the single-center CCC calculation. The dominant inelastic process is positronium formation for energies under 25 eV, excitation from 25 to 31 eV, and direct ionization for energies above 31 eV. There are no previous measurements or calculations to which the total inelastic cross section can be compared.

6. Frozen-core model

In this section, we investigate the importance of including non-frozen-core configurations in the structure calculations by comparing the present CCC calculations with CCC calculations utilizing a frozen-core model. In Fig. 9 we compare the 943-state CCC TCS and TICS with results obtained from a frozen-core 248-state CCC model which contains only the $2s^2 2pn\ell$ configuration continuum, with $n = 18 - \ell$ and $\ell_{\max} = 8$. As previously mentioned, the single-center

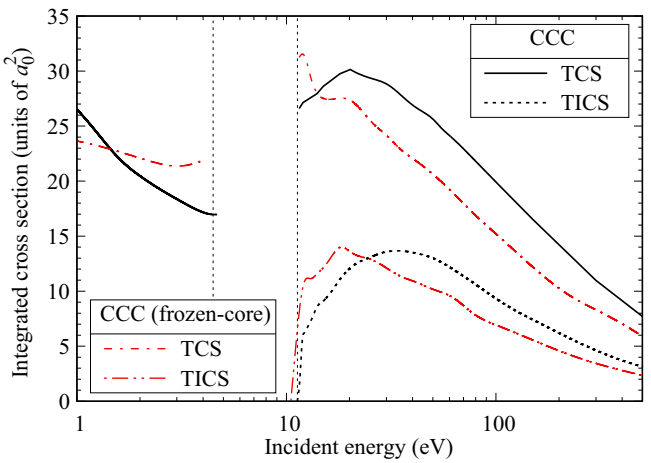

FIG. 9. Comparison of total cross section and total ionization cross section between 248-state frozen-core CCC model and 943-state CCC model. Results are presented from 1 to 500 eV.

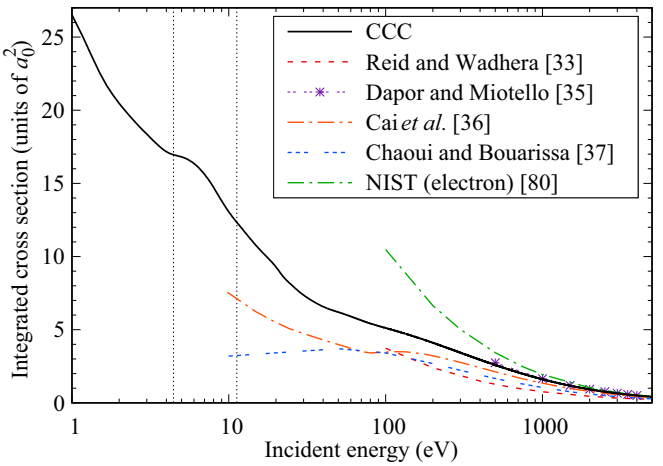

FIG. 10. Elastic scattering cross-section results for a positron scattering on carbon. CCC results are compared with the theoretical results of Reid and Wadehera [33], Dapor and Miotello [35], Cai *et al.* [36], and Chaoui and Bouarissa [37]. Also shown are the NIST elastic cross-section results for the electron case [80]. The vertical lines represent the positronium-formation and ionization thresholds. Note that between these thresholds the single-center calculation does not yield convergent results.

method is unstable between the positronium-formation and ionization thresholds due to mismatched boundary conditions. Therefore, results are not presented for this energy region in this figure. Between the ionization threshold and 14 eV, the frozen-core TCS sharply decreases, whereas the 943-state cross section softly increases. These differences are likely a result of the frozen-core approach not being stable at energies so close to the ionization threshold. Above 14 eV, the frozen-core model underestimates the TCS by up to 25%. The same is true for the TICS results above 20 eV. However, below this, the frozen-core model predicts a higher TICS cross section with a sharper peak. The differences below the positronium-formation energy between the two models can largely be ascribed to the insufficient number of available states in the frozen-core model resulting in a dipole polarizability value of 9.44 a_0^3, which is 23% lower than in the 943-state model.

Another significant discrepancy between these two models is that the frozen-core approach predicts an ionization threshold at 10.5 eV, which is almost 10% lower than our 943-state calculation. This discrepancy also extends to excitation energies, with the first excitation having a difference of 10% in its threshold; for each subsequent excitation, this difference consistently increases. From these observations, it is clear that the frozen-core structure model is insufficient for this system, and non-frozen-core configurations are necessary to obtain accurate results, particularly below the positronium-formation energy.

7. Elastic

In Fig. 10, the single-center CCC elastic cross section is compared with the theoretical calculation of Reid and Wadehra [33], Dapor and Miotello [35], Cai *et al.* [36], Chaoui and Bouarissa [37], and results obtained for the electron case from the NIST electron elastic-scattering

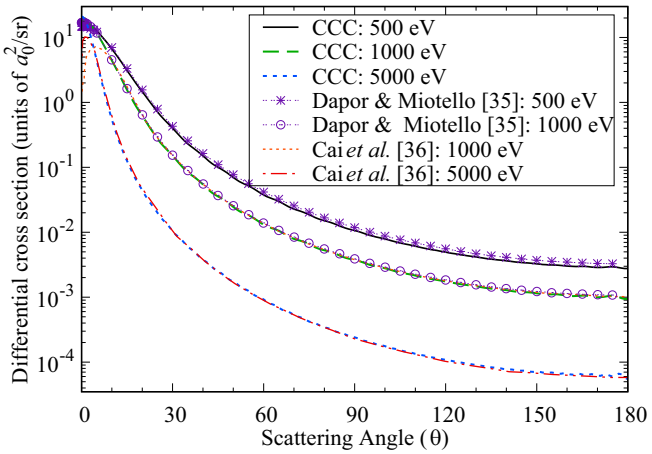

FIG. 11. Elastic scattering differential cross-section results for a positron incident upon carbon at 500, 1000, and 5000 eV. CCC results are presented against the theoretical results of Dapor and Miotello [35] and Cai *et al.* [36].

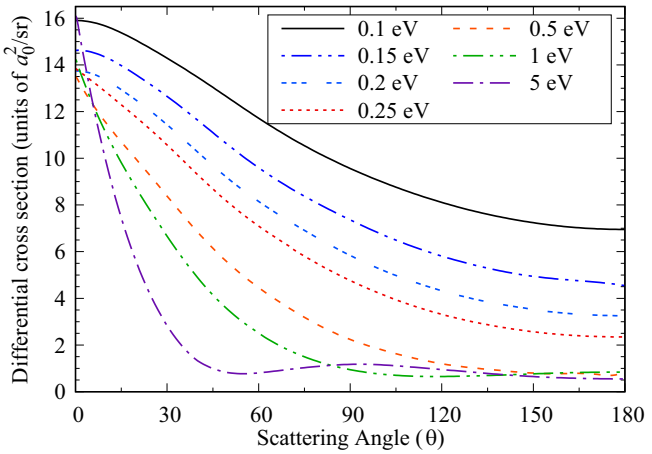

FIG. 12. CCC elastic scattering differential cross-section results for a positron incident upon carbon at 0.1, 0.2, 0.25, 0.5, 1, and 5 eV.

cross-section database [80]. For energies below the positronium-formation and above the ionization threshold, the single-center CCC will converge to the true result; however, the calculation is unstable between these energies. To address these instabilities in the $\ell_{\max} = 8$ calculation, the CCC results between 6 and 11.26 eV are taken from an $\ell_{\max} = 4$ calculation. As the single-center calculation cannot yield converged results for this energy range, the structure present within this range is likely a result of these instabilities and not a physical occurrence. Differences between the CCC calculation and those of Reid and Wadehra [33] are similar to those in the total cross section, with their results underestimating CCC over their entire energy range. The results of Cai *et al.* [36] agree with CCC above 2000 eV but are significantly lower for energies below this. This calculation also predicts a dip in the cross section at 80 eV, which is not seen in the CCC calculation. The calculations of Chaoui and Bouarissa [37] are between the calculations of Cai *et al.* [36] and Reid and Wadehra [33] for energies above 150 eV, while below this energy they predict a lower cross section than CCC and Cai *et al.* [36]. The calculations of Dapor and Miotello [35] are in excellent agreement with the CCC results over their calculated energy range of 500 to 4000 eV. The electron results from NIST agree with CCC results above 2000 eV, a much higher energy for electron and positron projectile agreement than in the total ionization cross-section case.

Differential cross sections for elastic scattering at incident energies of 500, 1000, and 5000 eV are presented in Fig. 11, alongside the calculations of Dapor and Miotello [35] and Cai *et al.* [36]. There is good agreement between the two calculations except for angles below 15° for 500 eV and 10° for 1000 eV. In both these cases, Cai *et al.* [36] predict a decrease in the DCS, whereas the CCC DCS has a maximum value at 0°. The calculations of Dapor and Miotello [35] are also in excellent agreement with the CCC results, and predict the same forward-scattering behavior as CCC. The calculations of Cai *et al.* [36] were performed with the ELSEPA [39] code, which performs Dirac partial-wave calculations for scattering systems. The method of Dapor and Miotello [35] also solved the Dirac equation but used a nonrelativistic Hartree-Fock potential for the target structure calculations.

In Fig. 12, we present a selection of CCC elastic DCS for incident energies between 0.1 and 5 eV. No previous calculations have been performed for these incident energies. Calculations were completed to ensure convergence in the partial-wave expansion, using a technique similar to Green *et al.* [81], which uses analytical properties of the long-range polarization potential. This allows us to describe the cusp present at low scattering angles for energies $\geqslant$1 eV. This feature is not present for lower energies as *p*-wave scattering is dominant for the triplet ground state of C.

8. Momentum transfer

A useful quantity for Monte Carlo and other simulations is the MTCS, which measures the average momentum transferred between the positron and C atom during the elastic scattering process. As with the elastic cross section, the CCC results between 6 and 11.26 eV are taken from an $\ell_{\max} = 4$ calculation. We present the results of our calculation alongside those of Dapor and Miotello [35] and Cai [38] in Fig. 13. We find excellent agreement between all calculations above 500 eV. Of the other theoretical methods, only Cai [38] performed calculations below 500 eV, and their calculation is slightly higher than CCC down to 30 eV, below which CCC predicts an increase in this cross section. An analysis of the low-energy behavior of this cross section is provided later.

9. Low-energy study

To demonstrate the impact of polarizability and virtual positronium formation on the elastic cross section and to enable calculation of the scattering length, we have calculated the elastic scattering cross section down to incident energies of 10^{-4} eV. Calculations were performed using three CCC models, the first being a single-state model in which the target polarizability is not accounted for, the second a model containing all 19 bound states which accounts for the major part of the polarizability but not virtual positronium formation, and lastly the full 943-state CCC model in which virtual positronium formation and polarizability are both fully accounted for. In Fig. 14, we compare the three models, which allows us to

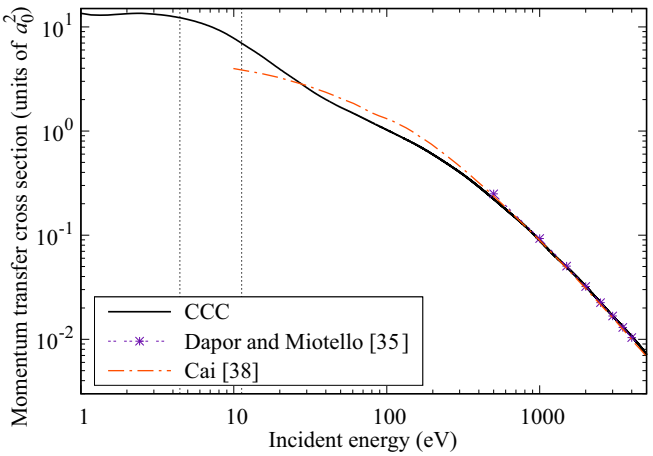

FIG. 13. Momentum transfer cross-section results for a positron incident upon carbon. CCC results are presented against the theoretical results of Dapor and Miotello [35] and Cai [38]. The vertical lines represent the positronium-formation and ionization thresholds. Note that between these thresholds the single-center calculation does not yield convergent results.

illustrate the effects of including various reaction channels. For the 943-state model, the elastic cross section rapidly rises and reaches an asymptotic value of 318 a_0^2. However, the single-state model is comparatively flat from 1 eV to lower energies, and the bound-state model decreases before reaching a constant value of 0.45 a_0^2.

From the asymptotic value of the 943-state low-energy elastic cross section, we can determine the scattering length via

$$\sigma_{\rm el} \approx 4\pi A^2, \tag{33}$$

where A is the scattering length [82]. Using this we obtain a scattering length for the e^+-C system of $A = \pm 5.03\, a_0$. To determine the sign, we can use [83]

$$\tan(\delta_0) = -Ak - \frac{\pi \alpha_{\rm D} k^2}{3a_0}, \tag{34}$$

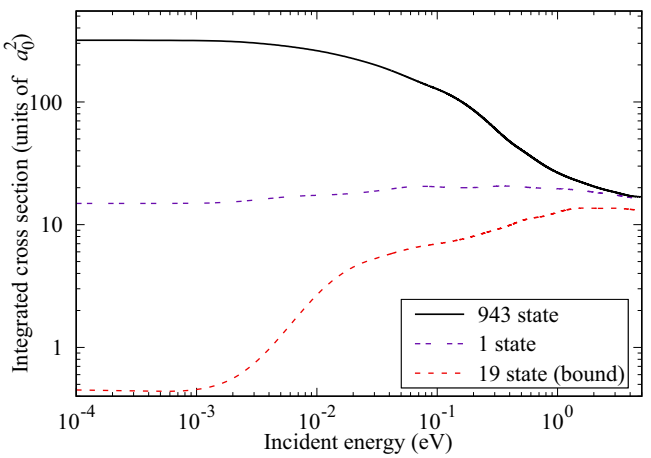

FIG. 14. Low-energy elastic scattering cross-section results for positron scattering on carbon. CCC results are presented for several different models from energies of 10^{-4} to 5 eV.

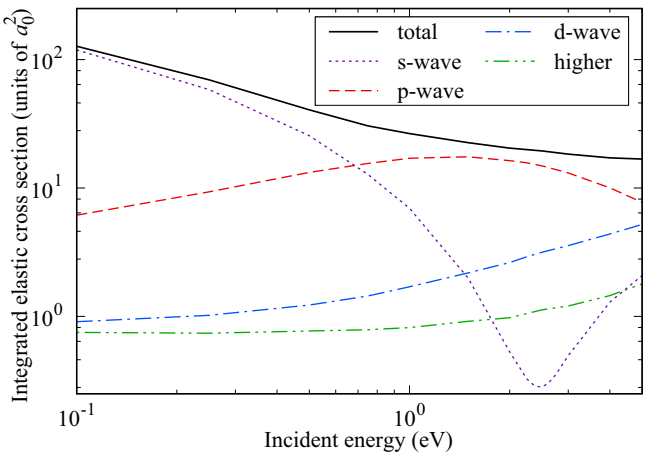

FIG. 15. Cross section for elastic total, s-, p-, d-, and higher-wave positron scattering from carbon for the energy range 0.1 to 5 eV.

where δ_0 is the s-wave phase shift. Using our δ_0 value at 10^{-4} eV we obtain $A = -5.03\, a_0$. The negative value indicates that this system has a strongly attractive nature at low energies [84]. The magnitude of A is larger than the mean radius of C, and the scattering cross section is much greater than the geometric size of the atom at low energies. This enhancement of the elastic cross section occurs due to the existence of a virtual level of the positron projectile [85], the energy of which can be obtained using

$$\epsilon = \frac{1}{2A^2}. \tag{35}$$

From our calculated A the energy of the e^+-C virtual state is found to be $\epsilon = 0.537$ eV.

As our scattering length is negative this implies the existence of a Ramsauer-Townsend minimum ($\rm RT_{min}$) which will occur at incident energy [86]

$$E_{\rm min} = \left(\frac{e^2}{2a_0}\right)\left(\frac{3|A|a_0^2}{\pi \alpha_D}\right)^2. \tag{36}$$

Using our calculated A and $\alpha_{\rm D}$ values we find $E_{\rm min}$ to be 2.34 eV. This $\rm RT_{min}$ occurs as a result of matter wave diffraction and appears in calculations when long-range polarization of the target by the incident projectile is taken into account [87]. Our integrated elastic cross section does not exhibit a minimum structure at this energy. However, it is observable when examining the s-wave contribution. This is shown in Fig. 15 alongside the p, d, and higher-ℓ contributions for 0.1 to 5 eV. It has been demonstrated in the literature that for positron scattering from noble gas atoms, the contributions of higher partial waves can result in the $\rm RT_{min}$ being hidden in the elastic cross section [81,88,89]. We observe this for carbon with the p, d, and higher-ℓ cross sections supplementing the decreased s-wave contribution. Over the energy range considered, we can see that s-wave scattering is dominant for incident energies below 0.6 eV. Above this, the p wave is dominant, with the peak p-wave cross section occurring at 1.5 eV. The $\rm RT_{min}$ we find in our integrated s-wave cross section occurs at an incident energy of approximately 2.45 eV, 0.11 eV higher than the value predicted by Eq. (36). This

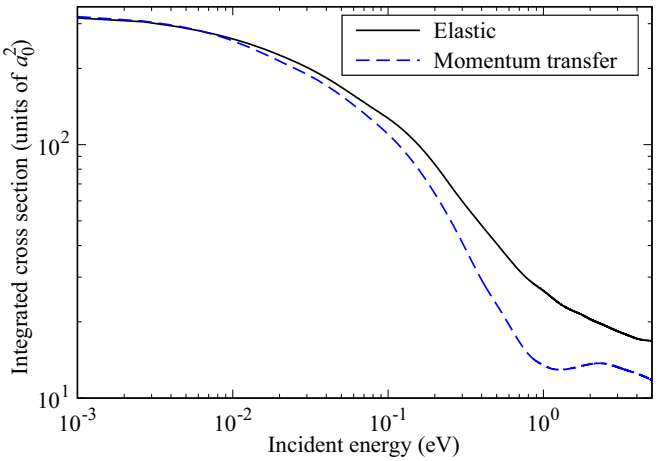

FIG. 16. Elastic and momentum transfer cross section for positron scattering from carbon for the energy range 10^{-3} to 5 eV.

difference is small and likely due to the omission of higher-order terms in Eqs. (33) and (34). From this difference, we can predict an uncertainty in our A of 2%.

Unlike the elastic cross section, in which the occurrence of a $\mathrm{RT}_{\mathrm{min}}$ solely depends on the s-wave phase shift, for the momentum transfer cross section, the presence of an $\mathrm{RT}_{\mathrm{min}}$ depends on the difference between the s- and p-wave phase shifts [88]. As a result, even with the $\mathrm{RT}_{\mathrm{min}}$ hidden in the elastic cross section, it can be present in the MTCS. This is the case for e^+-C scattering, where a minimum can be observed at approximately 1.25 eV in Fig. 16. The elastic and momentum transfer cross sections become equal when energies are low enough that scattering is isotropic, which our calculations predict to occur at energies below 0.01 eV.

10. Excitations

Cross sections for several excitations from the $2s^22p^2\ ^3P$ carbon ground state are presented in Fig. 17. The oscillator strengths for the $2p3d\ ^3D^o$ and $2s2p^3\ ^3P^o$ transitions had differences over 20% with the results of NIST. We have therefore scaled the positron-impact CCC cross section by the ratio between these oscillator strengths and those of NIST for these excitations, a process we refer to as OOS scaling. The scaled and unscaled results for these transitions are presented in the figure. As results for these excitations are unstable below the ionization threshold, these calculations have been linearly interpolated between their threshold and the ionization threshold. Since there are no previous positron-impact results for these processes, our results are presented alongside electron-impact scattering calculations. Due to the different scattering dynamics for positron and electron projectiles, the results are only expected to be equal at high energies, typically greater than 500 eV [63,90,91]. As results for these excitations have only been calculated to a maximum of 150 eV for electron impact, comments can only be made regarding general differences between our positron-impact calculation and the electron-impact calculations.

For these excitations positron-impact CCC results are typically closer in magnitude with the 696-state electron-impact BSR calculations [21] than other electron calculations, a reflection of our closer agreement in oscillator strengths. As expected, differences largely decrease with increasing energy between the BSR and CCC results, particularly in the $2s2p^3\ ^3D^o$ and $2s2p^3\ ^3P^o$ excitations. After scaling of the $2p3d\ ^3D^o$ excitation with the NIST oscillator strengths, we find our positron-impact results to be closer in magnitude to the CC [26] and BSR electron-impact models.

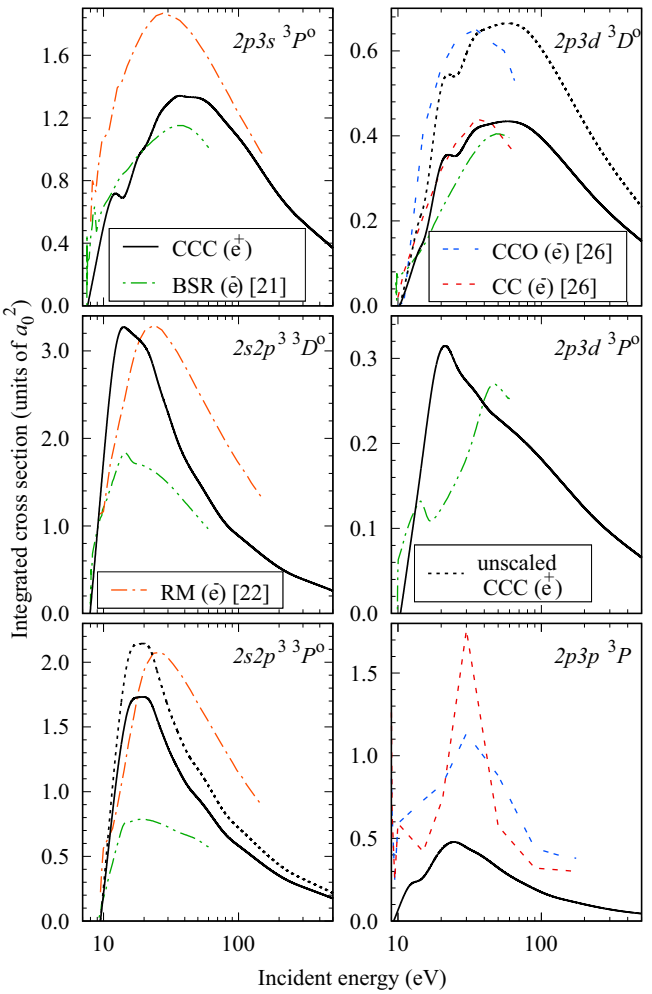

FIG. 17. Cross section for excitations from the ground state of carbon to several excited states from threshold to 500 eV. Positron-impact CCC results are shown alongside electron-impact calculations from the BSR [21] (—·—), R-matrix (RM) [22] (—··—), CCO [26] (— — —), and CC [26] (— — —) methods. For CCC results which have been OOS scaled, the unscaled result is shown by (……) and the scaled by (——).

Our positron-impact CCC results for the $2s2p^3\ ^3S^o$ autoionizing-state excitation from the ground state can be viewed in Fig. 18 with previous theoretical electron-impact results for this excitation. We have included results for a positron-impact model in which excitations from $2s2p^2n\ell$ were bound to $n\ell \leqslant 5s$, denoted as CCC (limited model). The results of this limited model are similar in magnitude to the electron-impact BEB [28] result at low energy and converge with it for energies above 2000 eV. The electron-impact R-matrix calculation of Dunseath *et al.* [22] is larger than both the BEB results and our CCC results above 25 eV. The

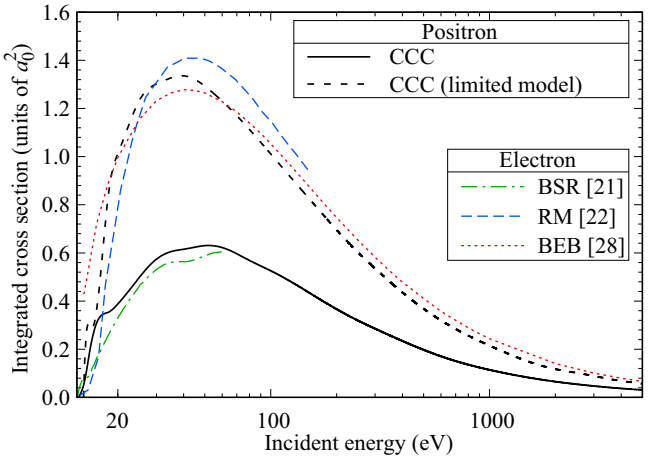

FIG. 18. Cross section of excitation from the ground state to the $2s2p^3\ ^3S^0$ autoionizing state. Positron-impact CCC and limited model CCC results are shown alongside electron-impact results calculated with BSR [21], R-matrix (RM) [22], and BEB [28] methods.

943-state CCC results are almost a factor of 2 lower than our limited model values and are larger than the BSR results up to 60 eV, where they appear to meet. The discrepancy between this calculation of Dunseath *et al.* [22] and the 943-state model is not surprising as their oscillator strength for this transition is almost twice the value we predict. Comparing our two CCC models, it is likely that the difference between the BSR and other electron-impact theoretical methods results from an inadequate description of the $2s2p^2n\ell$ continuum in the other approaches.

11. Stopping power and mean excitation energy

In Fig. 19, we present the stopping power, calculated from the ionization threshold to 5000 eV using Eq. (16). Alongside the CCC results are those from the Gumus *et al.* [42], PENELOPE program [44], and Ashley [45]. As was done for

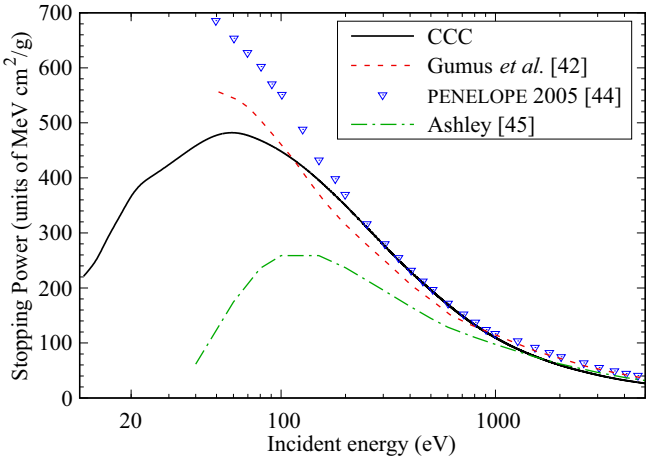

FIG. 19. Stopping power of a positron incident on carbon. CCC results are compared against those of Gumus *et al.* [42], the PENELOPE 2005 program [44], and Ashley [45]. These results are presented from the ionization threshold to 5000 eV.

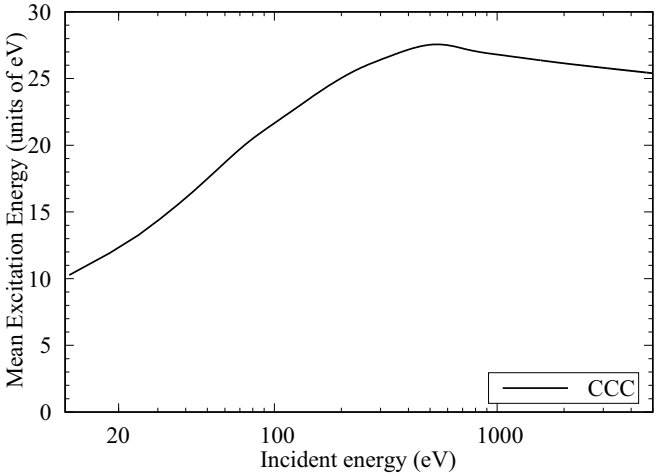

FIG. 20. Mean excitation energy of a positron scattering on carbon. Results are presented from the ionization threshold to 5000 eV.

ionization, the results were extrapolated using our 4571 Born calculation for energies above 50 eV. In these results, we cannot utilize the CCC-pot approach as it does not calculate the cross section for each specific excitation. Therefore, positronium formation is only included implicitly. From 250 to 1000 eV, there is excellent agreement between the CCC and PENELOPE results. Below 250 eV, the PENELOPE results are significantly higher than the CCC, with a difference of approximately 200 MeV cm^2/g at 50 eV, whereas above 1000 eV, the PENELOPE result is only slightly larger than the CCC. The PENELOPE program is a Monte Carlo program that calculates stopping power using a plane-wave Born approximation with the Sternheimer-Liljequist generalized oscillator strength model [92]. Therefore, the large differences at low energies are not surprising as this approach becomes increasingly inaccurate for energies below 1000 eV [44]. The results of the GOS model agree with PENELOPE for energies above 800 eV. Below this, the GOS model has lower values than both these models, except for energies below 100 eV, where it is larger than the CCC results. The calculations of Ashley [45] follow a similar shape to the CCC calculation but underestimate all other theoretical results below 1500 eV. Above this energy, however, there is excellent agreement with the CCC results.

The other theoretical approaches applied to stopping power are simpler methods that do not directly model the target structure of the atom or account for positronium formation. Therefore, while accurate for high energies, with all models practically equivalent above 1500 eV, they will be inaccurate at lower energies where scattering is more complex. As a result of the accurate structure model, the large number of included states, and the implicit inclusion of positronium formation, the CCC method is expected to model stopping power over the considered energy range more accurately than these other methods.

Following directly from the stopping power, we can obtain the mean excitation energy per Eq. (17). We present our results from the ionization threshold to 5000 eV in Fig. 20. We can observe that our mean excitation energy steadily increases to 500 eV, after which it plateaus and slowly decreases to

5000 eV. We could not find any other calculations of mean excitation energy for the e^+-C system in the literature.

V. CONCLUSION

Cross sections associated with the total, elastic, momentum transfer, direct ionization, positronium-formation, total ionization, inelastic, excitation, and stopping power scattering processes have been calculated for positron scattering on carbon over energies ranging from thresholds to 5000 eV. Several quantities of interest have also been determined. These include the scattering length, the energy of the virtual positron-carbon state, and the hidden Ramsauer-Townsend minimum. These calculations were completed using the single-center CCC approach utilizing different computational techniques, which have allowed us to extend calculations to complex open-shell atoms and ions. The calculated target wave functions are in good agreement with NIST and previous theory for oscillator strengths and excitation energies. For the single-center CCC method, results are practically exact below the positronium-formation threshold and above approximately 10 eV above the ionization threshold. Between these energies, the single-center approach is unable to fully account for the positronium-formation channels. Furthermore, the single-center approach can only obtain the sum of the positronium-formation and direct ionization cross section. To address these issues, we have introduced a complex model potential technique calibrated to accurate single-center results (CCC-pot), which allows us to calculate the relevant cross sections more accurately. An approach like this has not been utilized in previous applications of the model potential technique.

The present results have been compared with existing experimental and theoretical results for both positron and electron scattering on atomic carbon. TCS, elastic, momentum transfer, and stopping power cross sections were all in good agreement with previous calculations at high energies. There are substantial differences between the theoretical cross sections for positron scattering at low energies. Previous theoretical results also significantly overestimate the TICS across almost the entire calculated energy range. Our calculations, however, are in excellent agreement with the existing electron-carbon experiment above 500 eV. The differences between positron and electron scattering are minimal for high energies, and their results become practically the same. The main source of the differences present between CCC TICS and previous model potential approach calculations [41] is the positronium-formation process, with the previous theory being a factor of 1.5 larger than our results at the maximum for this cross section. It is recommended that further theoretical and experimental work is conducted for positron scattering on carbon to address the discrepancies highlighted by this study between current and past theoretical results. The CCC cross-section data for positron scattering from carbon are available at [93].

ACKNOWLEDGMENTS

The authors gratefully acknowledge the help of Dr. O. Zatsarinny, who provided assistance with the structure code used in this project. This research was supported by the Australian Government through the Australian Research Council's *Discovery Projects* funding scheme (Project No. DP190101195). HPC resources were provided by the Pawsey Supercomputing Research Centre with funding from the Australian Government and the Government of Western Australia. N.A.M. acknowledges the contribution of an Australian Government Research Training Program Scholarship.

APPENDIX A: CCC-SCALED COMPLEX MODEL POTENTIAL: HYDROGEN ATOM CALCULATION

To demonstrate the efficacy of the CCC-scaled complex model potential approach, we present calculations for positron scattering from the hydrogen atom for which both single- and two-center CCC results are available. We first obtain the complex model potential results utilizing the same approach as described in Sec. III. To summarize, we fit the polarization potential parameter d in our polarization potential given in Eq. (20) to obtain elastic cross sections equal to the single-center CCC for each energy. Between the positronium-formation and the ionization thresholds we instead fit to a line smoothly connected between these two thresholds. This is because the single-center approach is unstable between these two thresholds; this instability can be viewed in Fig. 22 as a large dip occurring at 10 eV. Elastic cross sections from our complex model potential are presented in Fig. 21 alongside single- and two-center CCC results. As expected, outside of the region between the positronium-formation and ionization thresholds, elastic results from the complex model potential are exactly equal to those of the single-center calculation. Our absorption potential is obtained following the method of Staszewska *et al.* [65], with values for the positronium-formation cross section obtained through the delta variational technique. With these positronium-formation values, we can obtain the direct inelastic cross section which is equal to the bound-state excitations summed with the direct ionization cross section. Hence, the total cross section contains three components: the direct inelastic cross section, the

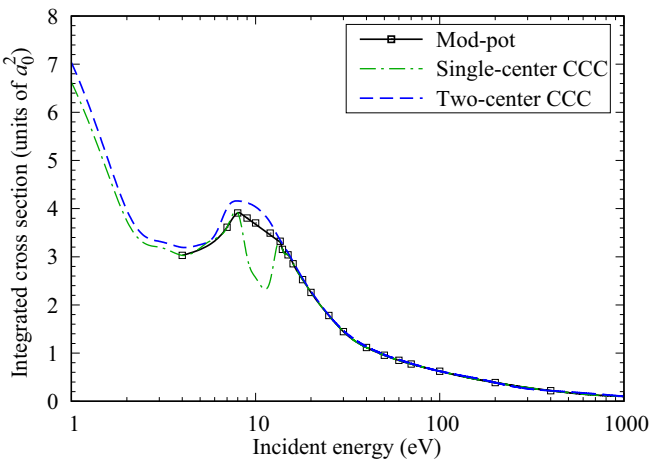

FIG. 21. Elastic cross section for positron scattering on the hydrogen atom. Single- and two-center CCC results are compared with the results obtained using the model potential.

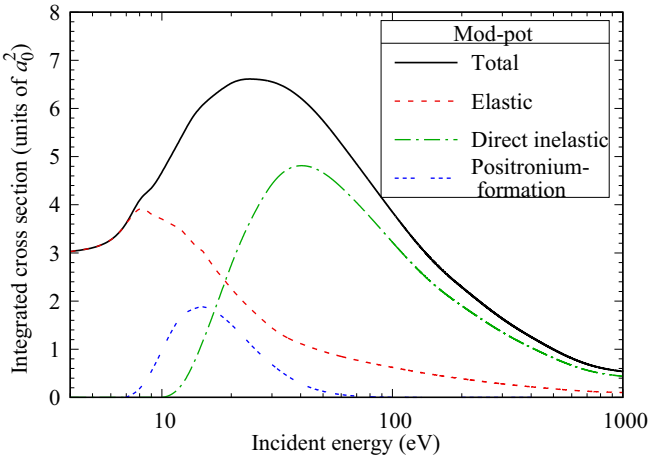

FIG. 22. The total cross sections and their components for the unscaled model potential calculation presented from the positronium-formation threshold to 1000 eV.

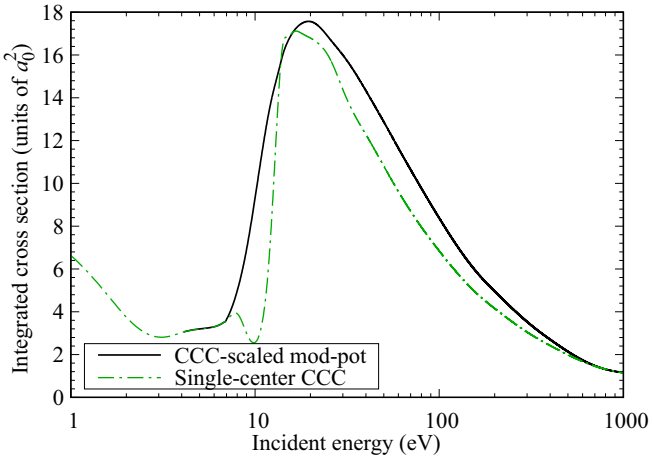

FIG. 24. CCC-scaled complex model potential and CCC single-center results for the positron-hydrogen total cross section. Here, the total cross section is comprised of the elastic, scaled direct inelastic, and scaled positronium-formation cross section.

positronium-formation cross section, and the elastic cross section. The total cross section of this unscaled complex model potential and its components are presented in Fig. 22. The first step of the CCC-scaling procedure is to scale the direct inelastic component of the total cross section to agree at large energies with the values predicted by the single-center CCC result. This is presented in Fig. 23, in which this component has been scaled by a factor of 2.4. Also shown are the single-center CCC results and the unscaled model potential.

The second step is to scale the positronium-formation component of the total cross section. We uniformly increase this cross section so that the CCC-scaled model potential total cross section reproduces the maximum single-center total cross section between the ionization threshold and 10 eV above the ionization threshold. For example, this occurs at 16 eV for hydrogen, so we scale the CCC-scaled model potential result to agree with the single-center CCC at 16 eV. In this case, the positronium-formation cross section was scaled by a factor of 5.75. The final results are depicted in Fig. 24, in which scaled positronium formation and inelastic results are summed with the elastic cross section to obtain the new total cross section. These results are again shown alongside corresponding single-center CCC results. The improvement in results from this scaling procedure is clear when comparing the unscaled results in Fig. 23 and the final scaled results in Fig. 24 to single- and two-center CCC results. The CCC-scaled model potential overestimates the single-center cross section for energies above 25 eV, resulting in inaccuracies in the CCC-scaled complex model calculation for the excitation cross section between 25 and 600 eV. As our subsequent calculations do not require these values, this is not considered an issue. By construction, the elastic cross section is equivalent to the single-center CCC results; therefore, this component does not require any scaling.

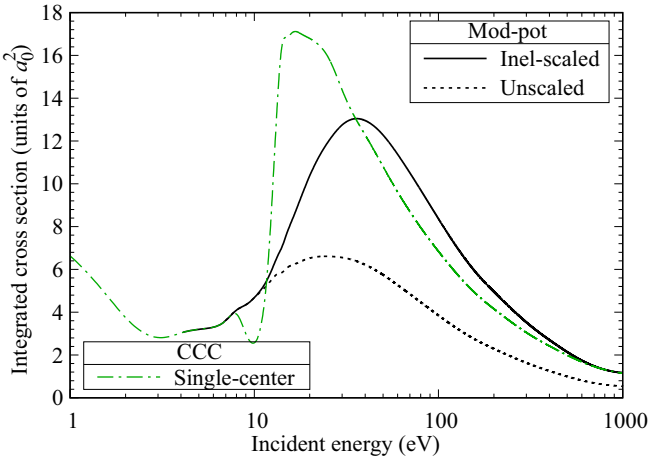

FIG. 23. Complex model potential total cross-section results for which direct inelastic cross sections have been scaled to agree with CCC results for larger energies. In these results positronium-formation cross sections are currently unscaled. These results are presented with the single-center CCC results.

We can directly compare the scaled positronium-formation cross section with the two-center CCC. We present this in Fig. 25, where it can be seen that our scaled result is both equal to and has the correct position of the peak cross section of the positronium formation. However, our calculation somewhat underestimates the two-center result for energies above and below this peak. We can obtain direct ionization results for energies 10 eV greater than the ionization energy by subtracting these values from the single-center total ionization cross section from our positronium-formation results. For energies below this point, we rely on the CSP-ic method. First, we obtain $R(E)$ values for energies 10 eV above ionization, and then we fit a spline interpolant to obtain the $R(E)$ for lower energies. We can obtain the direct ionization cross section by multiplying these fitted values by the direct inelastic cross section obtained from our CCC-scaled complex model potential. More details of this procedure can be found in Sec. III. The calculated and fitted $R(E)$ results are depicted in Fig. 26. These results rise to a maximum of approximately 0.55 at 50 eV before dropping to an asymptote of approximately 0.4

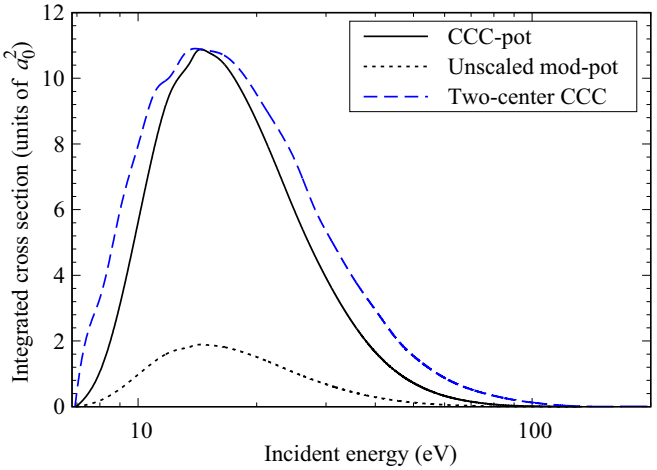

FIG. 25. Hydrogen positronium-formation cross section for our unscaled and CCC-scaled complex model potential presented with two-center CCC results for energies ranging from the positronium-formation threshold to 200 eV.

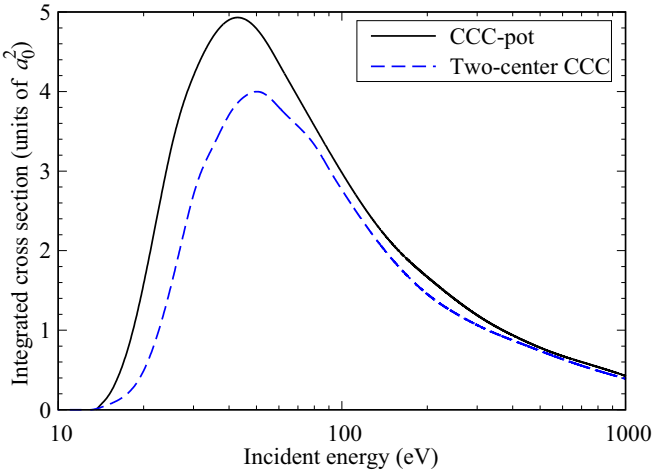

FIG. 27. Hydrogen direct ionization cross section for our unscaled and CCC-scaled complex model potential presented with two-center CCC results.

by 1000 eV. This represents that by 1000 eV 40% of the direct inelastic cross section is composed of direct ionization.

In Fig. 27, we present our results for direct ionization obtained using the CCC-scaled complex model potential approach and those obtained via the two-center CCC. We can observe that differences between these methods mainly occur for energies less than 75 eV, which directly results from the errors in our positronium-formation calculation. The peak of this approach overestimates the two-center CCC, with differences within 25%. For lower energies, particularly near the ionization threshold, we find larger differences; however, the magnitude of the cross section at these energies is small.

We have direct ionization and positronium-formation results and can now calculate the total ionization cross section. This is calculated from the summation of our scaled positronium-formation and direct ionization cross sections with these results presented in Fig. 28 alongside single- and two-center CCC results. The benefit of our approach compared to the single-center CCC is clear with our results in significantly better agreement with the two-center calculation from positronium-formation threshold to 10 eV above the ionization threshold. Below the ionization threshold, the differences between CCC-pot and the two-center calculation are the same as for the positronium formation. Whereas, from the ionization threshold to 10 eV above it, the differences are within 5%.

The excitation cross section can also be calculated using the direct ionization cross section. For energies higher than 10 eV above the ionization threshold, we use $\sigma_{\rm exc} = \sigma_{\rm tot} - \sigma_{\rm Ps} - \sigma_{\rm DI} - \sigma_{\rm el}$ where $\sigma_{\rm tot}$ is from our single-center CCC result. For energies below this, we do the same but use $\sigma_{\rm tot}$ from our CCC-scaled complex model potential calculation. The total bound excitation cross section is shown in Fig. 29 alongside single- and two-center CCC results. We can observe that this approach is a great improvement over the single center for lower energies, where instabilities in the

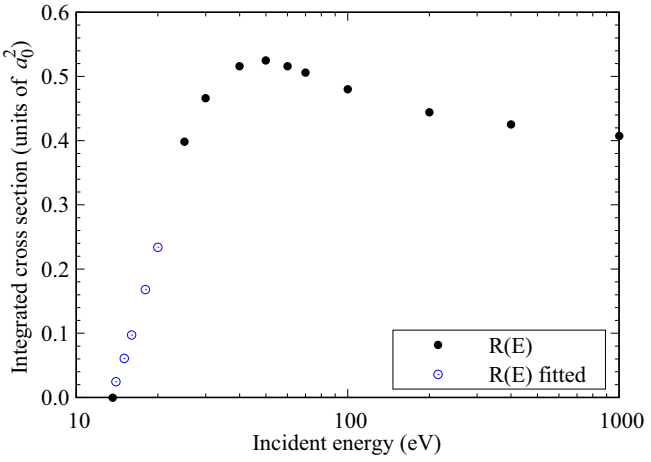

FIG. 26. Calculated $R(E)$ and fitted $R(E)$ values for positron scattering from hydrogen.

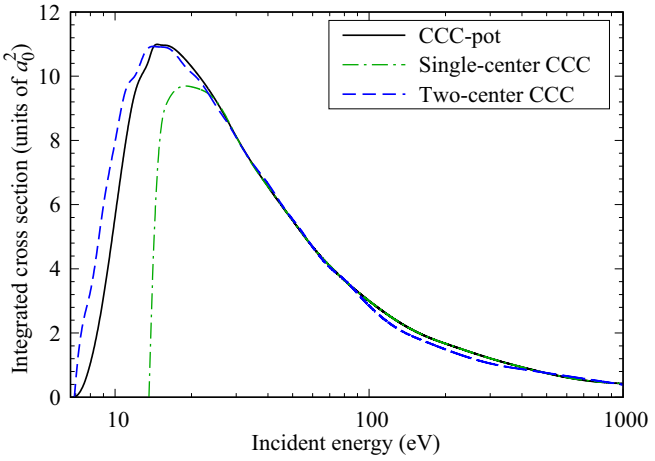

FIG. 28. Hydrogen total ionization cross section from our approach presented with single- and two-center CCC results. Results are presented from the positronium-formation threshold to 1000 eV.

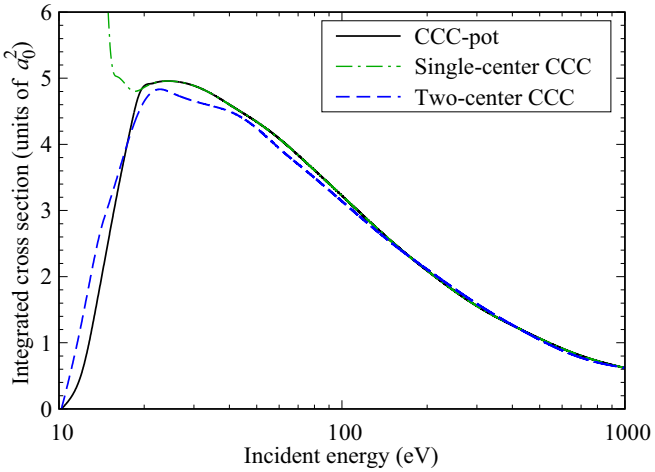

FIG. 29. Total excitation cross section for hydrogen calculated from our approach alongside single- and two-center CCC results.

single-center calculation for energies near the ionization threshold have resulted in substantially larger results than the two-center calculation. We find differences between this approach and the two-center calculation to be within 5%.

Finally, for the calculation of the total cross section, we now combine the results of the single-center and CCC-scaled model potential. For this, we use our single-center results for energies below the positronium formation and higher than 10 eV above the ionization threshold. For energies between the positronium-formation threshold and 10 eV above ionization, we use the total cross section calculated by the CCC-scaled model potential. We have compared these results with the single- and two-center CCC results for hydrogen in Fig. 30. We find that results are significantly improved from the single-center CCC calculation for the energies between the positronium-formation and ionization thresholds. Results still underestimate the two-center CCC over this energy range, with our results within 20% of the two-center results. From the ionization threshold to 10 eV above this threshold, errors between our results and the two-center CCC are within 10%.

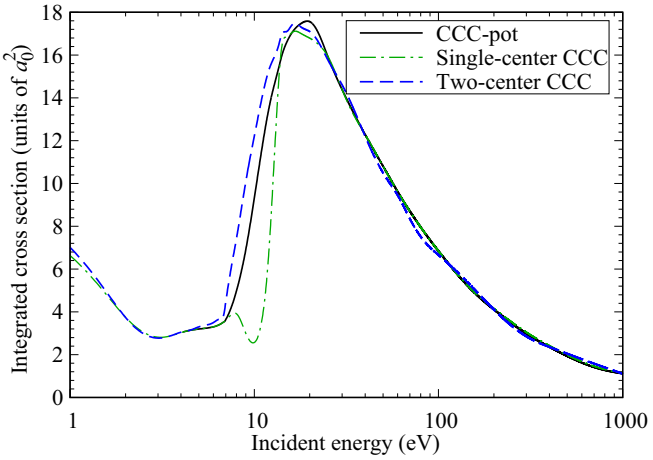

FIG. 30. Combined results for the hydrogen total cross section alongside single- and two-center CCC results.

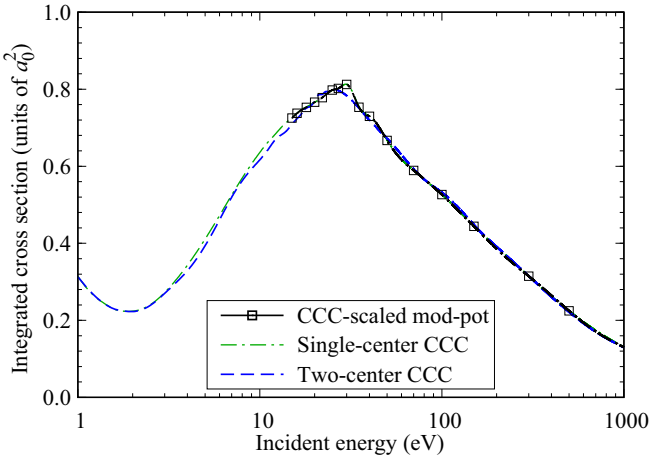

FIG. 31. Elastic cross section for positron scattering on the helium atom. Single- and two-center CCC results are compared with the results obtained using the model potential.

APPENDIX B: CCC-SCALED COMPLEX MODEL POTENTIAL: HELIUM ATOM CALCULATION

As we have already depicted the process of the CCC scaling of the direct inelastic and positronium-formation cross sections for the hydrogen model potential calculation, we only present the final results for the helium atom. Model potential calculations are undertaken following the same process described in Sec. III and Appendix A. As with hydrogen, smooth elastic cross sections were obtained using a line fit between the positronium-formation and ionization thresholds. These elastic cross sections are presented in Fig. 31 alongside single- and two-center CCC results. First, we present CCC-scaled model potential total cross-section results in Fig. 32 alongside single-center CCC results. For this model, the direct inelastic component was scaled by a factor of 1.51 and the positronium-formation component by a factor of 6.71. For helium, the maximum cross section for the single-center calculation occurs at 70 eV, a much higher energy than is observed in the hydrogen case.

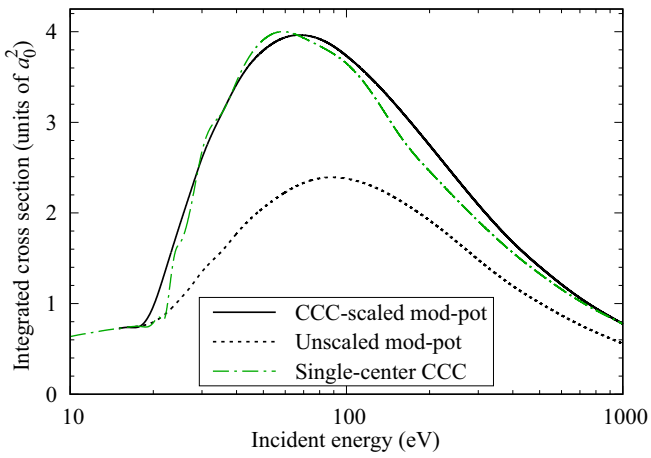

FIG. 32. CCC-scaled complex model potential, unscaled complex model potential, and CCC single-center results for the positron-helium total cross section.

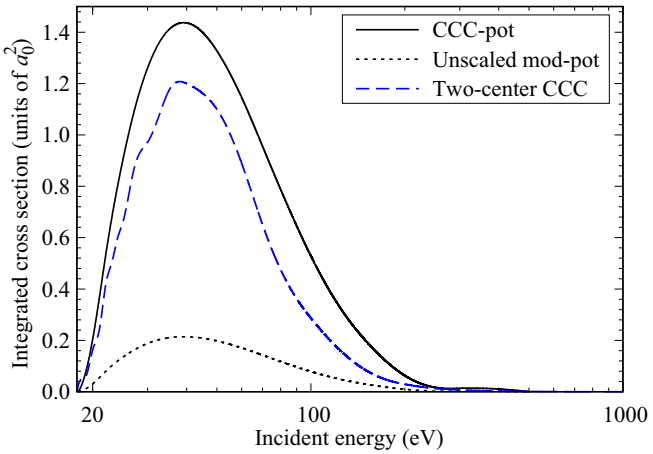

FIG. 33. Helium positronium-formation cross sections for our unscaled and CCC-scaled complex model potential presented with two-center CCC results. Results are presented from the positronium-formation threshold to 1000 eV.

Presented in Fig. 33 are positronium-formation cross sections for the CCC-scaled complex model potential, unscaled complex model potential, and two-center CCC results. Model potential calculations were completed as described in Sec. III with scaling applied to the direct inelastic and positronium-formation cross sections as described in Sec. III and Appendix A. Unlike hydrogen, our results overestimate the two-center results across the entire energy range. These results are within 20% of the two-center results for results up to 50 eV. As with hydrogen, the energy of our peak cross section is the same as the two-center calculation.

In Fig. 34, we present the direct ionization result for this approach against the two-center CCC results. As with hydrogen, we find that as a result of errors in the positronium formation, our direct ionization overestimates at lower energies and the peak cross section. We also find that the peak cross section occurs at the same energy between both methods at 100 eV. There exists less error here than with hydrogen,

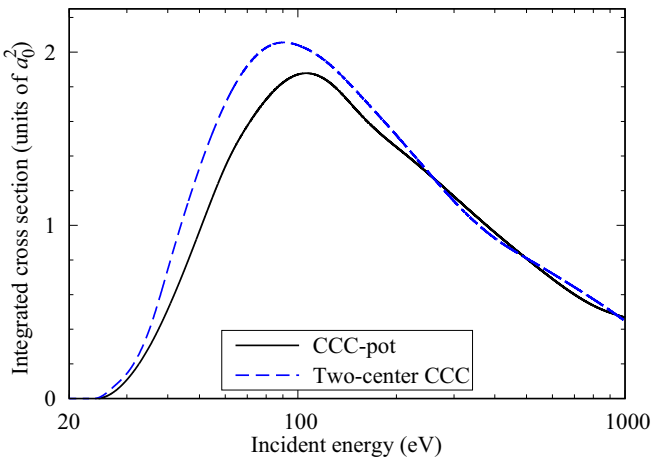

FIG. 34. Helium direct ionization cross section for our unscaled and CCC-scaled complex model potential presented with two-center CCC results.

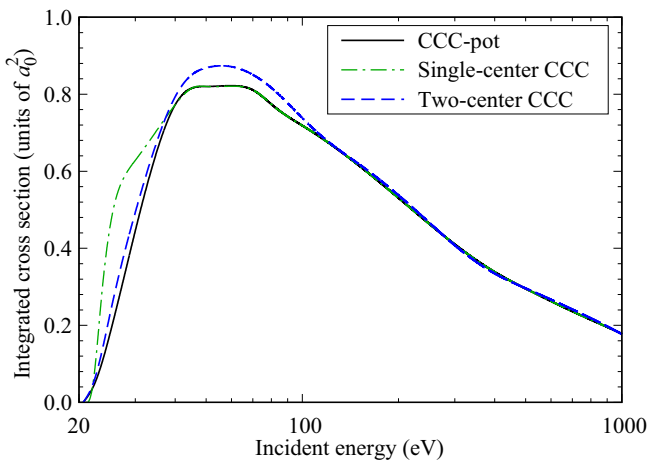

FIG. 35. Total excitation cross section for helium calculated from our approach alongside single- and two-center CCC results.

with all values within 20% of the two-center CCC result. We also find much better agreement for energies below this peak cross section than was viewed with hydrogen, likely because the positronium formation has a much lower magnitude for helium.

We have also used our method to calculate the total excitation cross section for a helium atom. This is shown in Fig. 35 with single- and two-center CCC results. We see significant improvement from the single-center results for energies below 10 eV above the ionization threshold, with the cross sections here having near perfect agreement with the two-center calculation.

Finally, in Fig. 36 we can find the combined results of the CCC-scaled complex model potential and single-center CCC alongside the single- and two-center CCC. As with hydrogen over the energy range between positronium formation and ionization, our results are a significant improvement over the single-center calculation. As the elastic cross section is scaled to be equivalent to the single-center CCC result, there is no point in calculating CCC-pot below the positronium-formation threshold, as the only process available below this

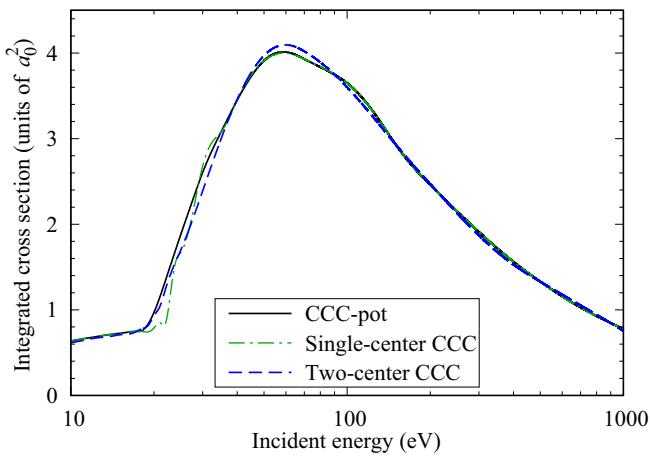

FIG. 36. Combined results for the helium total cross section alongside single- and two-center CCC results.

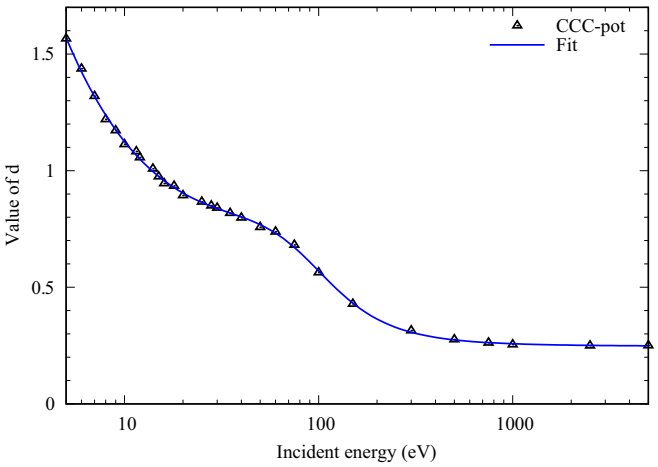

FIG. 37. Value of the parameter d required to achieve equivalence with single-center CCC calculation for positron scattering on atomic carbon. Results are presented from 5 to 5000 eV.

threshold is elastic scattering. Here we find even better agreement than was found with hydrogen, with our total cross sections having errors of 5% or lower over this energy range. From the ionization threshold to 10 eV above this threshold, we find similar errors with results within 5%, again an improvement from hydrogen.

APPENDIX C: ERROR ANALYSIS AND LIMITATIONS OF CCC-SCALED COMPLEX MODEL POTENTIAL

The accuracy of this approach and the improvement it provides for single-center CCC calculations for both the hydrogen and helium targets is promising. It justifies its application to other targets, as these two targets have very different scattering behaviors, polarization potentials, and ionization, excitation, and positronium-formation thresholds. Following analysis of these systems, we expect positronium formation to have an accuracy of 20% for energies up to three times the ionization threshold from this method. Above this, the difference between this and the two-center results increases with increasing energy. Although these results are not particularly accurate for the highest considered energies due to the low magnitude of these results, they can still be utilized to calculate sufficiently accurate direct ionization cross sections.

For direct ionization, we expect the peak cross section to be within 20% of the two-center value, with energies below this having higher inaccuracies if the positronium-formation cross section is significantly larger than the direct ionization. For higher energies, where the positronium-formation cross section is small, we expect the accuracy for this cross section to be within 5%. For the total excitation cross section, we expect an error of 5%. Across the energy range in which the CCC-scaled complex model potential is utilized for the total cross section, we expect the errors to be within 20%.

Limitations for this approach are that we require the maximum of the total cross section to occur after the ionization threshold to find reasonable estimates for the positronium-formation cross section. Hence, in conjunction with accurate single-center CCC results, we expect this method to obtain sufficiently accurate results for atoms with ionization energies greater than 10 eV.

TABLE III. Fit parameters.

i	p_i	q_i
1	0.2473	−74.57
2	−10.66	7336
3	3822	4224
4	4.528×10^4	

APPENDIX D: POLARIZATION POTENTIAL MODIFICATION PARAMETER

We show in Fig. 37 the parameter d utilized in Eq. (20), for incident energies 5 to 5000 eV of a positron upon the carbon atom. This is shown alongside a fit of the form

$$f(e) = \frac{(p_1e^3 + p_2e^2 + p_3e + p_4)}{e^3 + q_1e^2 + q_2e + q_3}, \tag{D1}$$

where e is the energy of the incident positron. The values of the fitting parameters are given in Table III. The value of the parameter d decreases with increasing energy up to 750 eV, after which it becomes constant.

[1] H. Watabe, Y. Ikoma, Y. Kimura, M. Naganawa, and M. Shidahara, Ann. Nucl. Med. **20**, 583 (2006).
[2] L. Menichetti, L. Cionini, W. A. Sauerwein, S. Altieri, O. Solin, H. Minn, and P. A. Salvadori, Appl. Radiat. Isot. **67**, S351 (2009).
[3] Y. F. Taia and P. Piccini, J. Neurol. Neurosurg. Psychiatry **75**, 669 (2004).
[4] Y. Wang, M. Li, R. Diao, B. Tung, D. Zhang, and Y. Li, Oncotarget **8**, 51652 (2017).
[5] V. Caridad, M. Arsenak, M. J. Abad, R. Martin, N. Guillen, L. F. Colmenter, and P. Taylor, Cancer Biother. Radiopharm. **23**, 371 (2008).
[6] S. Fang, J. Wang, H. Jiang, Y. Zhang, W. Xi, C. Zhao, M. Tian, and H. Zhang, Cancer Biother. Radiopharm. **25**, 733 (2010).
[7] R. M. Moadel, R. H. Weldon, E. B. Katz, P. Lu, J. Mani, M. Stahl, M. D. Blaufox, R. G. Pestell, M. J. Charron, and E. Dadachova, Cancer Res. **65**, 698 (2005).
[8] D. M. Paul, C. M. Ghiuzeli, J. Rini, C. J. Palestro, E. K. Fung, M. Ghali, E. Ben-Levi, A. Prideaux, S. Vallabhajosula, and E. C. Popa, Am. J. Nucl. Med. Mol. Imaging **10**, 334 (2020).
[9] C. Makochekanwa, A. Bankovic, W. Tattersall, A. Jones, P. Caradonna, D. S. Slaughter, K. Nixon, M. J. Brunger, Z. Petroivc, J. P. Sullivan, and S. J. Buckman, New J. Phys. **11**, 103036 (2009).
[10] C. Champion and C. Le Loirec, Phys. Med. Biol. **52**, 6605 (2007).
[11] L. Jødal, C. L. Loirec, and C. Champion, Phys. Med. Biol. **57**, 3931 (2012).

[12] N. Mott and H. Massey, *The Theory of Atomic Collisions* (Oxford University Press, Oxford, 1966).
[13] H. Massey and E. Burhop, *Electronic and Ionic Impact Phenomena* (Oxford University Press, Oxford, 1969).
[14] F. Blanco and G. García, Phys. Lett. A **317**, 458 (2003).
[15] F. Blanco, L. Ellis-Gibbings, and G. García, Chem. Phys. Lett. **645**, 71 (2016).
[16] D. Liljequist, T. Liamsuwan, and H. Nikjoo, Int. J. Radiat. Biol. **88**, 29 (2012).
[17] P. Helander and D. J. Ward, Phys. Rev. Lett. **90**, 135004 (2003).
[18] T. Fülöp and G. Papp, Phys. Rev. Lett. **108**, 225003 (2012).
[19] J. Liu, H. Qin, N. J. Fisch, Q. Teng, and X. Wang, Phys. Plasmas **21**, 064503 (2014).
[20] O. Zatsarinny, K. Bartschat, L. Bandurina, and V. Gedeon, Phys. Rev. A **71**, 042702 (2005).
[21] Y. Wang, O. Zatsarinny, and K. Bartschat, Phys. Rev. A **87**, 012704 (2013).
[22] K. M. Dunseath, W. C. Fon, V. M. Burke, R. H. G. Reid, and C. J. Noble, J. Phys. B: At., Mol. Opt. Phys. **30**, 277 (1997).
[23] V. Stancalie, J. Phys.: Conf. Ser. **576**, 012010 (2015).
[24] S. A. Abdel-Naby, C. P. Ballance, T. G. Lee, S. D. Loch, and M. S. Pindzola, Phys. Rev. A **87**, 022708 (2013).
[25] K. Joshipura and P. Patel, Z. Phys. D **29**, 269 (1994).
[26] J. Liu, Y. Wang, and Y. Zhou, J. Phys. B: At., Mol. Opt. Phys. **39**, 861 (2006).
[27] R. J. W. Henry, P. G. Burke, and A. L. Sinfailam, Phys. Rev. **178**, 218 (1969).
[28] Y.-K. Kim and J.-P. Desclaux, Phys. Rev. A **66**, 012708 (2002).
[29] P. M. Stone and Y. S. Kim, Surf. Interface Anal. **37**, 966 (2005).
[30] M. S. Pindzola, J. Colgan, F. Robicheaux, and D. C. Griffin, Phys. Rev. A **62**, 042705 (2000).
[31] E. Brook, M. F. A. Harrison, and A. C. H. Smith, J. Phys. B: At. Mol. Phys. **11**, 3115 (1978).
[32] K. I. Wang and C. K. Crawford, EIectron impact ionization cross sections particle optics lab, MIT Technical Report, 1971 (unpublished).
[33] D. D. Reid and J. Wadehra, Chem. Phys. Lett. **311**, 385 (1999).
[34] F. B. Malik, Z. Naturforsch. Pt. A. **16**, 500 (1961).
[35] M. Dapor and A. Miotello, At. Data Nucl. Data Tables **69**, 1 (1998).
[36] L. H. Cai, B. Yang, C. C. Ling, C. D. Beling, and S. Fung, J. Phys.: Conf. Ser. **262**, 012009 (2011).
[37] Z.-E.-A. Chaoui and N. Bouarissa, J. Appl. Phys. **96**, 807 (2004).
[38] L. Cai, Induced secondary electrons in thin carbon foils, M.Phil. thesis, University of Hong Kong, Pokfulam, Hong Kong, 2010.
[39] F. Salvat, A. Jablonski, and C. J. Powell, Comput. Phys. Commun. **165**, 157 (2005).
[40] S. Singh, S. Dutta, R. Naghma, and B. Antony, J. Phys. Chem. A **120**, 5685 (2016).
[41] S. Singh and B. Antony, Europhys. Lett. **119**, 50006 (2017).
[42] W. Gumus, T. Namdar, and A. Bentabet, Int. J. Mol. Biol. Open Access **3**, 87 (2018).
[43] ICRU, Stopping powers for electrons and positrons, Technical Report (International Commission on Radiation Units and Measurements, 1984).
[44] F. Salvat, J. Fernández-Varea, and J. Sempau., Penelope, a code systems for Monte Carlo simulation of electron and photon transport, France: NEA Databank, 2005.
[45] J. Ashley, J. Electron Spectrosc. Relat. Phenom. **50**, 323 (1990).
[46] I. Bray and A. T. Stelbovics, Phys. Rev. A **48**, 4787 (1993).
[47] J. J. Bailey, A. S. Kadyrov, and I. Bray, Phys. Rev. A **91**, 012712 (2015).
[48] A. S. Kadyrov and I. Bray, Phys. Rev. A **66**, 012710 (2002).
[49] R. Utamuratov, A. S. Kadyrov, D. V. Fursa, and I. Bray, J. Phys. B: At., Mol. Opt. Phys. **43**, 031001 (2010).
[50] R. Utamuratov, A. S. Kadyrov, D. V. Fursa, I. Bray, and A. T. Stelbovics, Phys. Rev. A **82**, 042705 (2010).
[51] H. Wu, I. Bray, D. V. Fursa, and A. T. Stelbovics, J. Phys. B: At., Mol. Opt. Phys. **37**, 1165 (2004).
[52] H. Wu, I. Bray, D. V. Fursa, and A. T. Stelbovics, J. Phys. B: At., Mol. Opt. Phys. **37**, L1 (2003).
[53] R. Utamuratov, D. V. Fursa, A. S. Kadyrov, R. I. Campeanu, and R. P. McEachran, Eur. Phys. J. D **75**, 260 (2021).
[54] A. V. Lugovskoy, A. S. Kadyrov, I. Bray, and A. T. Stelbovics, Phys. Rev. A **85**, 034701 (2012).
[55] A. V. Lugovskoy, A. S. Kadyrov, I. Bray, and A. T. Stelbovics, Phys. Rev. A **82**, 062708 (2010).
[56] A. V. Lugovskoy, R. Utamuratov, A. S. Kadyrov, A. T. Stelbovics, and I. Bray, Phys. Rev. A **87**, 042708 (2013).
[57] R. Utamuratov, D. V. Fursa, A. S. Kadyrov, A. V. Lugovskoy, J. S. Savage, and I. Bray, Phys. Rev. A **86**, 062702 (2012).
[58] D. V. Fursa and I. Bray, J. Phys.: Conf. Ser. **388**, 012020 (2012).
[59] O. Zatsarinny, Comput. Phys. Commun. **174**, 273 (2006).
[60] C. F. Fischer, Comput. Phys. Commun. **64**, 369 (1991).
[61] R. Utamuratov, A. S. Kadyrov, D. V. Fursa, M. C. Zammit, and I. Bray, Phys. Rev. A **92**, 032707 (2015).
[62] A. S. Kadyrov and I. Bray, J. Phys. B: At., Mol. Opt. Phys. **49**, 222002 (2016).
[63] N. A. Mori, R. Utamuratov, L. H. Scarlett, D. V. Fursa, A. S. Kadyrov, I. Bray, and M. C. Zammit, J. Phys. B: At., Mol. Opt. Phys. **53**, 015203 (2019).
[64] M. C. Zammit, D. V. Fursa, and I. Bray, Phys. Rev. A **87**, 020701(R) (2013).
[65] G. Staszewska, D. W. Schwenke, and D. G. Truhlar, Chem. Phys. **81**, 335 (1984).
[66] I. Bray and A. T. Stelbovics, Phys. Rev. A **46**, 6995 (1992).
[67] L. H. Scarlett, J. S. Savage, D. V. Fursa, I. Bray, M. C. Zammit, and B. I. Schneider, Phys. Rev. A **103**, 032802 (2021).
[68] R. Utamuratov, D. V. Fursa, N. Mori, A. S. Kadyrov, I. Bray, and M. C. Zammit, Phys. Rev. A **99**, 042705 (2019).
[69] K. Haris and A. Kramida, Astrophys. J. Suppl. Ser. **233**, 16 (2017).
[70] F. Salvat, Phys. Rev. A **68**, 012708 (2003).
[71] L. Chiari, A. Zecca, S. Girardi, E. Trainotti, G. García, F. Blanco, R. P. McEachran, and M. J. Brunger, J. Phys. B: At., Mol. Opt. Phys. **45**, 215206 (2012).
[72] I. Bray and A. T. Stelbovics, Comput. Phys. Commun. **85**, 1 (1995).
[73] S. Singh and B. Antony, J. Appl. Phys. **121**, 244903 (2017).
[74] https://www.nist.gov/.
[75] A. Das and A. J. Thakkar, J. Phys. B: At., Mol. Opt. Phys. **31**, 2215 (1998).
[76] P. Schwerdtfeger and J. K. Nagle, Mol. Phys. **117**, 1200 (2019).
[77] G. F. Gribakin and W. A. King, J. Phys. B: At., Mol. Opt. Phys. **27**, 2639 (1994).
[78] V. Jonauskas, Astron. Astrophys. **620**, A188 (2018).
[79] Y.-K. Kim, Phys. Rev. A **64**, 032713 (2001).

[80] A. Jablonski, C. J. Powell, and A. Y. Lee, NIST electron elastic-scattering cross-section database version 4.0, NIST standard reference database number 64, https://srdata.nist.gov/srd64/.
[81] D. G. Green, J. A. Ludlow, and G. F. Gribakin, Phys. Rev. A **90**, 032712 (2014).
[82] A. Zecca, L. Chiari, E. Trainotti, D. V. Fursa, I. Bray, A. Sarkar, S. Chattopadhyay, K. Ratnavelu, and M. J. Brunger, J. Phys. B: At., Mol. Opt. Phys. **45**, 015203 (2012).
[83] T. F. O'Malley, Phys. Rev. **130**, 1020 (1963).
[84] R. P. McEachran, A. G. Ryman, and A. D. Stauffer, J. Phys. B: At. Mol. Phys. **12**, 1031 (1979).
[85] C. M. Surko, G. F. Gribakin, and S. J. Buckman, J. Phys. B: At., Mol. Opt. Phys. **38**, R57 (2005).
[86] D. D. Reid and J. M. Wadehra, J. Phys. B: At., Mol. Opt. Phys. **47**, 225211 (2014).
[87] P. G. Burke, *Potential Scattering in Atomic Physics* (Plenum, New York, 1977).
[88] F. Arretche, M. V. Barp, W. Tenfen, and E. P. Seidel, Braz. J. Phys. **50**, 844 (2020).
[89] V. Dzuba, V. Flambaum, G. Gribakin, and W. King, J. Phys. B: At., Mol. Opt. Phys. **29**, 3151 (1996).
[90] C. C. Montanari and J. E. Miraglia, J. Phys. B: At., Mol. Opt. Phys. **48**, 165203 (2015).
[91] G. Karwasz, Eur. Phys. J. D **35**, 267 (2005).
[92] M. Asai, M. A. Cortés-Giraldo, V. Giménez-Alventosa, V. Giménez Gómez, and F. Salvat, Front. Phys. **9**, 660 (2021).
[93] See Supplemental Material at http://link.aps.org/supplemental/10.1103/PhysRevA.107.032817 for CCC positron-carbon scattering cross sections.